2021-02

Role of Future Reef Growth on Morphological Response of Coral Reef Islands to SeaLevel Rise

Masselink, Gerd

http://hdl.handle.net/10026.1/17962

Role of Future Reef Growth on Morphological Response of Coral Reef Islands to Sea-Level Rise

G. Masselink[1], **R. McCall[2]**, **E. Beetham[3]**, **P. Kench[4]**, and **C. Storlazzi[5]**

[1]School of Biological Sciences, Coastal Processes Research Group, University of Plymouth, Plymouth, UK, [2]Deltares, Delft, The Netherlands, [3]Tonkin and Taylor International Ltd., Auckland, New Zealand, [4]Department of Earth Sciences, Simon Fraser University, Burnaby, BC, Canada, [5]Pacific Coastal and Marine Science Center, USGS, Santa Cruz, CA, USA

Abstract Coral reefs are widely recognized for providing a natural breakwater effect that modulates erosion and flooding hazards on low-lying sedimentary reef islands. Increased water depth across reef platforms due sea-level rise (SLR) can compromise this breakwater effect and enhance island exposure to these hazards, but reef accretion in response to SLR may positively contribute to island resilience. Morphodynamic studies suggest that reef islands can adjust to SLR by maintaining freeboard (island crest elevation above still water level) through overwash deposition and island accretion, but the impact of different future reef accretion trajectories on the morphological response of islands remains unknown. Here we show, using a process-based morphodynamic model, that, although reef growth significantly affects wave transformation processes and island morphology, it does not lead to decreased coastal flooding and island inundation. According to the model, reef islands evolve during SLR by attuning their elevation to the maximum wave runup and islands fronted by a growing reef platform attain lower elevations than those without reef growth, but have similar overwash regimes. The mean overwash discharge Q_{over} across the island crest plays a key role in the ability of islands to keep up with SLR and maintain freeboard, with a Q_{over} value of $O\,(10\,\text{l}\,\text{m}^{-1}\,\text{s}^{-1})$ separating island construction from destruction. Islands, therefore, can grow vertically to keep up with SLR via flooding and overwash if specific forcing and sediment supply conditions are met, offering hope for uninhabited and sparely populated islands. However, this physical island response will negatively impact infrastructure and assets on developed islands.

Plain Language Summary Coral reef islands are particularly exposed to the impacts of sea-level rise. They are usually fronted by "living" coral reef platforms that protect the island shoreline from energetic wave action. Healthy reef platforms grow vertically and can keep up with rising sea level, maintaining a constant water depth in front of the island. It is therefore suggested that future reef growth may be a critical factor in reducing the vulnerability of coral reef islands to sea-level rise. We use a computer model to simulate the response of coral reef islands to sea-level rise with and without future reef growth. We find that as sea level rises, the islands evolve by retreating, while at the same time building up vertically. Island build-up is accomplished by waves overwashing the island and depositing sediment on the top of the island. According to our model results, vulnerability of the reef islands to sea-level rise is not dependent on whether the reef platform grows or not. In both cases, islands are regularly overwashed, but this is necessary for islands to grow vertically. Island accretion by overwash offers hope for uninhabited and sparely populated islands, but will negatively impact infrastructure and assets on urbanized islands.

1. Introduction

Coral reef islands are wave-built accumulations of carbonate sediment deposited on sub-horizontal reef platforms with a reef edge that slopes steeply to deeper water. They tend to have a surface area $O\,(0.1–1\,\text{km}^2)$ with their long axis oriented parallel to the prevailing wave direction, and they can be densely vegetated or developed with infrastructure. A characteristic feature of these islands is their low-lying nature (<4 m above mean sea level), which makes them susceptible to coastal flooding and island inundation during extreme events, such as cyclones (Scoffin, 1993), long-period wave events (Wadey et al., 2017) and tsunamis (Kench et al., 2006). Of particular concern to the communities living on these islands is the increased

probability of wave-driven flooding due to future sea-level rise (SLR) and possibly increased storminess, and it is widely assumed that the islands will become increasingly uninhabitable through this century (Storlazzi et al., 2018), threatening the very existence of the coral reef island nations (Duvat & Magnan, 2019). However, these pessimistic outlooks are based on both the reef platform and the island being geologically inert structures, and disregard two important processes that may positively contribute to island resilience to SLR.

First, coral reefs that host reef islands are presently sea-level limited, with a reef flat elevated around low tide or mean sea level. Future SLR will open accommodation space for vertical reef accretion (Perry et al., 2012; Woodroffe & Webster, 2014), which could limit a net increase in reef depth and therefore wave energy at island shorelines (Beetham et al., 2017). Reef growth is likely to be compromised in many reef regions as a consequence of climate change stressors and direct anthropogenic impacts (Hoegh-Guldberg, 1999; Hughes et al., 2017; Pandolfi et al., 2011; van Woesik et al., 2015). However, coral colonization on reef flats and net reef accretion has been measured on some reefs experiencing relative SLR (Brown et al., 2011; Saunders et al., 2016; Scopélitis et al., 2011), suggesting that reef accretion in response to future SLR is still possible under the right conditions. The potential for vertical reef growth to keep pace with SLR is likely to be spatially variable and is contingent on the existing reef health and the trajectory of future climate change stressors (Perry et al., 2018; Ryan et al., 2019; van Woesik and Cacciapaglia, 2018, 2019).

Second, similar to all coastal morphodynamic systems (e.g., salt marshes, mangroves, and barrier systems), coral reef islands can respond or adjust morphologically to SLR through sediment transport. Recent physical (Tuck, Ford, et al., 2019; Tuck, Kench, et al., 2019) and numerical (Masselink et al., 2020) modeling has demonstrated that overwash processes can result in island accretion and raising of the crest level. The frequency of this process will be enhanced by SLR and is also associated with retreat of the island shoreline. Such conclusions are supported by field evidence documenting washover deposition on island surfaces in response to a range of wave driven mechanisms (Kench et al., 2006; Kench & Beetham, 2019; Hoeke et al., 2013). This "roll-over" response is well documented in gravel (e.g., Orford et al., 1995) and sand (e.g., Carruthers et al., 2013) barrier field studies, and barrier modeling studies (Lorenzo-Trueba & Ashton, 2014), and is characterized by the migration of the barrier (or island) through erosion of the ocean shoreline and deposition at the back of the barrier (or island) and/or the lagoon shoreline. A complicating factor affecting overwash hydrodynamics on sand barriers is the presence of aeolian dunes (Houser, 2013), but this is rarely a factor on gravel barriers or coral reef islands, where dunes are generally absent. It is also important to consider that offshore sediment losses may occur on sandy barrier islands under extreme wave conditions, but these are unlikely to occur in reef island settings where the presence of a wide and horizontal reef flat inhibits the development of strong offshore-directed currents. A key concept emerging from barrier studies is that of the difference in height between the elevation of the barrier crest and the maximum runup level, termed "overwash potential" (Matias et al., 2012, 2016) or "freeboard" (Orford et al., 2003; Sallenger, 2000). The response of barriers to elevated wave and water levels is shown to be strongly determined by the amount and sign of this height difference. In the coastal engineering literature, the term "freeboard" is, however, more commonly used to denote the difference in elevation between the crest of a structure or barrier and the still water level (EurOtop, 2018), and this is the definition used throughout this paper. In common with barrier systems, the response of reef islands to SLR depends on a range of *forcing* factors (rate of SLR, changes in the storm wave climate) and *controlling* factors (sediment supply, island geometry, reef platform topography) with freeboard playing a key role.

Reef platforms that surround islands are generally considered to play a key role in protecting islands from erosion and flooding as they dissipate incident ocean wave energy and control residual energy reaching the shoreline (Cheriton et al., 2016; Ferrario, 2014). Increased sea levels will fundamentally change this protective role and modify the receipt of wave energy at shorelines, potentially exposing islands to increased shoreline erosion and island flooding (Beetham & Kench, 2018; Beetham et al., 2017; Quataert et al., 2015; Storlazzi et al., 2011). Critical factors governing the energy incident at island shorelines are the still water depth across the platform h_{reef} and the width of the platform w_{reef}, and both have been explored using the BEWARE data set (Pearson et al., 2017). This data set was generated with the nonhydrostatic version of the process-based XBeach model (McCall et al., 2014; Smit et al., 2010) by exposing a set of idealized reef platforms and island configurations to a wide range of forcing conditions to investigate wave runup and wave-induced flooding (Figure S1). These model data demonstrate that the incident wave height at the toe

of the beach and the wave runup, and thus the risk of wave-induced flooding, increases with water depth across the platform (cf., Beetham et al., 2017; Pearson et al., 2017; Quataert et al., 2015), while the infragravity wave height at the toe of the beach and the wave setup increases with decreased water depth across the platform (cf., Masselink et al., 2018).

It can thus be surmised that if the reef platform vertically accretes at the same rate as SLR (h_{reef} = constant), the protective role of the platform will be maintained, but if the platform surface does not keep up (h_{reef} increases), greater water depths across the platform will expose the reef island to increasingly energetic conditions (Cheriton et al., 2016; Beetham et al., 2017; Quataert et al., 2015). However, the reef platform is not the only feature that may evolve during SLR, as the reef island may also adjust (Tuck, Ford, et al., 2019; Tuck, Kench, et al., 2019). The aim of this study is therefore to explore the role of reef platform growth on the ability of coral reef islands to morphodynamically adjust to SLR under energetic wave conditions (H_0 = 3 m). We follow a similar modeling approach as Masselink et al. (2020), but extend the analysis by considering the response of both gravel and sand islands, accounting for reef growth and modeling SLR of up to 2.5 m, and also considering the impact of moderate (H_0 = 2 m) to extreme (H_0 = 5 m) wave conditions.

2. Materials and Methods

2.1. Morphodynamic Modeling Using XBeach-G

The XBeach-G (McCall et al., 2015, 2014) numerical model, which is the 1DH, phase-resolving, gravel version of the XBeach model that accounts for groundwater interactions, was used in this study. This modeling approach was selected because it is a well-established process-based morphodynamic model with the ability to deal with wave overtopping and infiltration effects that are essential to coral reef island morphodynamics. Most aspects of the model have been extensively validated at the lab and field scale: (1) phase-resolving wave hydrodynamics in reef environments (Lashley et al., 2018; Pearson, et al., 2017; Quataert et al., 2020); (2) groundwater interactions (McCall et al., 2014); and (3) morphological response of gravel (McCall et al., 2015) and mixed sand-gravel (Bergillos, et al., 2017) barriers to storms.

The ability of the phase-resolving XBeach model to simulate overwash processes on sandy barriers has not been tested yet. However, the phase-averaged XBeach model (Roelvink et al., 2009), which was specifically developed for modeling sand barrier response to extreme events, has been very comprehensively tested using field data (Harter & Figlus, 2017; Lindemer et al., 2010; McCall et al, 2010; Passeri et al., 2018; Smallegan et al., 2016; Van der Lugt et al., 2019). Attempts to model the morphodynamics of coral reef islands using a phase-resolving version of XBeach have been limited. Using phase-averaged bed load transport formulations in combination with phase-resolved hydrodynamics, Pomeroy and Van Rooijen (2019) found the model able to generally reproduce observed beach slope change, but not the berm development observed in flume experiments. Masselink et al. (2020) improved upon this by applying the intra-wave bed load transport model of XBeach-G to simulate beach and berm morphodynamics, and used small-scale laboratory modeling to validate the numerical model.

Sediment transport in the version of XBeach-G used here is modeled using a standard Shields approach:

$$q_s = 12(\theta - 0.05)\sqrt{\theta}\sqrt{\left(\frac{\rho_s - \rho}{\rho}\right)gD_{50}^3},$$

(1)

where q_s = volumetric sediment transport rate (m^3 s^{-1}), θ = Shields parameter (−), ρ and ρ_s = density of water and sediment (kg m^{-3}), respectively, and D_{50} is the median grain diameter (m). The Shields parameter is adjusted for bed slope effects:

$$\theta = \frac{u_*^2}{\left((\rho_s - \rho) / \rho\right)gD_{50}}\cos(\beta)\left(1 \pm \frac{\tan(\beta)}{\tan(\phi)}\right),$$

(2)

where $u_* =$ friction velocity (m s^{-1}), $\beta =$ bed angle (°) and $\phi =$ angle of repose of the sediment (°). To account for boundary layer expansion and contraction in the swash, pressure gradient effects, and the presence of turbulent fronts, following Nielsen (2002), the friction velocity is computed using the approximation:

$$u_* = \sqrt{\frac{f_s}{2}} \left(\cos(\varphi) u + \frac{T_{m-1,0}}{2\pi} \sin(\varphi) \frac{\delta u}{\delta t} \right), \tag{3}$$

where $f_s =$ user-defined sediment friction factor (0.01 was used here), $T_{m-1,0} =$ offshore spectral period based on the first negative moment of the energy spectrum (s) and φ is a user-defined phase lag angle (30° was used here). The phase angle φ in this approach is critical as it represents the phase lag between the free-stream velocity and the bed shear stress, and values larger than 0 increasingly promote the onshore transport of sediment. The equation was specifically developed to model horizontally asymmetric wave motion (such as in surf zone bores, swash and overwash) which is known to drive sediment onshore.

Calibration/validation of a morphodynamic model generally relies on "tuning" only a small number of coefficients and Masselink et al. (2020) demonstrated that "realistic" coral reef island response can be achieved through various combinations of only three parameters (sediment size D_{50}, the phase angle φ and hydraulic conductivity K; see Equations 1–3). Specifically, they demonstrated (cf., their Figure 2 and Table 2) using model simulations forced with $H_s = 4$ m, that parameter combinations [$D_{50} = 6$ mm, $\varphi = 30°$, $K = 0.005$ m s^{-1}], [$D_{50} = 10$ mm, $\varphi = 25°$, $K = 0.01$ m s^{-1}], [$D_{50} = 12$ mm, $\varphi = 25°$, $K = 0.005$ m s^{-1}] and [$D_{50} = 15$ mm, $\varphi = 25°$, $K = 0$ m s^{-1}] all provided very similar results. In addition, they found that combinations of $D_{50} < 8$ mm and $\varphi < 25°$ resulted in offshore sediment transport across the seaward-facing part of the island and ultimately island destruction.

For the schematic modeling approach used here, where *idealized* reef island topographies are used to provide insight into how changing a single forcing or controlling factor (e.g., reef platform growth vs. no reef platform growth, rapid SLR vs. slow SLR, sand vs. gravel, etc.) modifies island response, we consider using XBeach-G with previously calibrated values for the key sediment transport parameters (Masselink et al., 2020) appropriate. However, for site-specific applications and the specific quantification of tipping-points, we would recommend separate model validation to take place. It is also important to consider that the sediment volume within the model domain was constant and determined by the initial island sediment volume, that is, no sediment was added by carbonate production nor lost off the platform to deeper water during the simulations.

2.2. Using Idealized Reef Platform and Island Topography

An initial XBeach model was set up (Figure 1a), characterized by an immovable, impermeable and smooth reef platform ($w = 700$ m; $z = 0$ m; depth-dependent $c_D \sim 0.03$) across the platform (cf., McCall et al., 2015), with steep (tan$\beta = 0.5$) reef slopes on both sides that terminate in a horizontal surface ($z = -25$ m). A permeable and movable island was placed on the platform with a width w of 300 m and 200 m at the base and top, respectively, and a crest height z_{crest} of 5 m and 4 m at the exposed ocean and lagoon shorelines, respectively. The associated ocean beachface, island-top and lagoon beachface slopes were 0.100, 0.005, and 0.080, respectively. The model grid resolution was set to vary according to the profile depth from 3.25 m at $z = -25$ to 0.25 m at $z = 0$ m to ensure sufficient resolution across the reef platform and island, while maintaining an optimal Courant-based numerical time step in the deeper sections of the model. The island was composed of either gravel or sand material, and the associated median sediment size D_{50} and hydraulic conductivity K were 0.014 m and 0.001 m, and 0.005 m s^{-1} and 0 m s^{-1}, respectively. The sand island was made impermeable to maximize the contrast with the gravel island to help bring out disparate behavior.

The platform-island topography used for the numerical modeling is considered characteristic of many atoll rim islands (e.g., Kench et al., 2017; Woodroffe, 2008) and examples of a typical gravel and sand coral reef island are shown in Figure S2. In common with the modeled platform-island topography, the natural reef islands have a 100–200 m wide, sub-horizontal reef platform at the ocean-side (Figure S2a, S2b, S2d, and S2e), a steeper gravel than sand beachface (Figure S2c and S2f) and an island elevation that is higher for the gravel than the sand island (3–5 m and 2–3 m above reef platform level, respectively; Figure S2a and S2d). However, the natural reef islands tend to be characterized by multiple ridges, whereas the modeled island
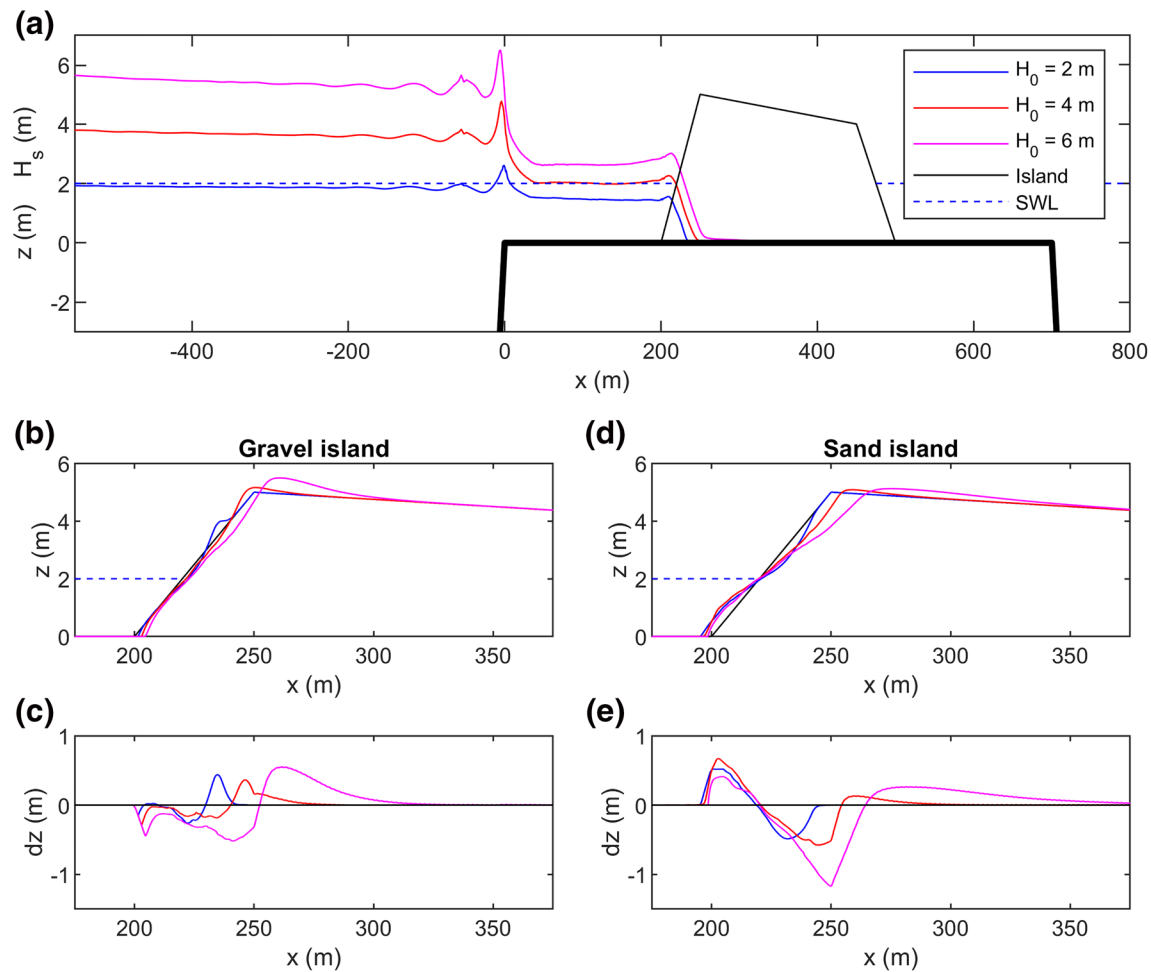
Figure 1. XBeach model results for varying wave forcing: (a) cross-shore variation in H_0 and general reef-island set-up; (b and c) profile evolution for different wave forcing for gravel island ($D_{50} = 14$ mm, $K = 0.005$ m s^{-1}; (d and e) profile evolution for different wave forcing for sand island ($D_{50} = 1$ mm, $K = 0$ m s^{-1}). $H_0 = 2$–6 m, $T_p = 9.9$ s, $h_{reef} = 2$ m and each model run lasted 3 h.

has a flat top. It is emphasized that every natural reef-island structure is unique and that the modeling was specifically designed to ignore site-specific idiosynchrasies (e.g., presence of beachrock) and that an idealized topography was used in the model to enable comparison between gravel and sand island response to SLR, and isolate the role of reef platform growth.

2.3. Selecting Appropriate Wave Forcing (Test A)

All models were forced with 1-h segments of wave forcing defined by a JONSWAP spectrum with a peak enhancement value of 3.3, and with instantaneous morphodynamic updating (XBeach model parameter "morfac = 1"). For all morphodynamic simulations (Sections 2, 3.1, 3.2, 3.4 and 3.5), hourly wave forcing varied stochastically ("instat = jons"), whereas for the hydrodynamic simulations (Sections 3.3) an identical wave forcing signal was used ("instat = reuse"). The overwash discharge is a key parameter controlling island response (Masselink et al., 2020). In the model simulations, time series of the water discharge were extracted for the island crest location and hourly averaged, and the average discharge rate Q_{over} is expressed in l m^{-1} s^{-1}. All simulations were done for gravel and sand, and an overview of all model runs is provided in Table S1.

To select the default wave and tide level conditions for the model simulations it was assumed that incremental island adjustment is primarily accomplished during conditions that just reach the island crest;

low-to-moderate wave hydrodynamic conditions only shape the island beach (Kench et al., 2017, 2009) and only extreme conditions result in large-scale transformation of the island structure. It is also assumed that conditions that significantly modify the top of the island are limited to high tide and/or extreme events when setup levels across the reef flat and shoreline are elevated, and this was considered to be at $z = 2$ m (resulting in a still water depth across the reef platform h_{reef} of 2 m). A peak wave period T_p of 9.9 s was used. A large number of 3-h test simulations were conducted with offshore significant wave heights increasing from $H_0 = 1$ m to 6 m in 0.5-m steps (**Test A**; Table S1). It was found that for $H_0 < 2.5$ m, wave runup did not reach the island crest and that for $H_0 > 3.5$ m, a large amount of overwashing occurred, significantly modifying both the gravel and sand island, and causing considerable crest accretion for the gravel island and crest retreat for the sand island (Figures 1b–1e). The associated across-reef variation in significant wave height H_s is displayed in Figure 1a and shows wave breaking at the reef edge followed by wave dissipation and wave setup across the reef platform. A value of $H_0 = 3$ m was used for simulations B–E as it represents the wave forcing that would lead to the development of the crest at an elevation approximately equal to that of the initial island profile. A value of $H_0 = 3$ m happens to reflect a wave height that roughly corresponds to the 1% exceedance wave height for portions of the tropical Pacific as modeled by the Changing Waves and Coasts in the Pacific project (WACOP.gsd.spc.int). It therefore reflects an energetic wave condition that can be expected to occur at high tide a few times per year in this region, but perhaps only once a year during spring high tide. Selection of such a "formative" wave condition is analogous to the concept of a bankful discharge in hydrology, where river channel characteristics (width, depth, cross-section) are related to the flow that reaches the transition between the channel and adjacent flood plain.

2.4. Priming Reef Island Morphology (Test B)

Although the elevation of the island broadly corresponds to the maximum runup associated with $H_0 = 3$ m, $T_p = 9.9$ s, $h_{reef} = 2$ m and $\tan\beta = 0.1$, the morphology of the front of the idealized island (i.e., the "beach-face") is unlikely to reflect the exact shape and position that is in equilibrium with those forcing conditions. To avoid "contaminating" the morphological response of the island to SLR by the morphological adjustments toward an equilibrium profile shape, the island morphology was "primed" by exposing the island profile to 50 h of wave conditions before raising the sea level. The "primed" island morphology was thus used as a starting point for the sea-level simulations (**Test B**; Table S1). Figure 2b and 2c shows the gravel and sand island morphology after 250 h of constant wave and water-level conditions ($H_0 = 3$ m, $T_p = 9.9$ s, $h_{reef} = 2$ m), and Figures 2d–2f shows time series of some key morphometric parameters: cumulative gross morphological change $\Sigma|dz|$, island crest elevation z_{crest} and island crest position x_{crest}. Figure 2a shows the associated wave and set-up profile across the reef platform.

The gravel island response to the "priming" period is characterized by onshore sediment transport, resulting in a steepening of the beachface from $\tan\beta = 0.1$ to 0.15 and the construction of a small berm (0.8 m high) at the original island crest position. Sediment transport on the sand island is offshore across the submerged part of the beachface and onshore in the swash zone, resulting in a flattening of the beachface from $\tan\beta = 0.1$ to 0.05, the construction of a small submerged bar and subaerial berm (0.9 and 0.2 m high, respectively), and 15 m retreat of the island crest. The gravel island response involves less cumulative gross change than on the sand island ($\Sigma|dz| = 100$ and 200 m^3 m^{-1}, respectively), but for both islands 75% of the total $\Sigma|dz|$ over the 250-h model simulations is accomplished during the first 50 h (Figure 2d), suggesting that equilibrium is being approached. This is also indicated by the overwash discharge Q_{over} at the crest location, which, on both types of islands, progressively decreases during the simulation from 0.5 l m^{-1} s^{-1} to insignificant (Figure 2g). Note that no further change can occur at the island crest if the overwash discharge approaches zero. The gravel and sand island morphology after 50 h of modeling is used as the "primed" profile for all sea-level simulations. It is acknowledged that this does not represent a "true" equilibrium—both islands will keep incrementally increasing their crest elevation as long as the steepening beachface results in increased wave runup elevation—but the rate of change after 50 h of constant sea level is an order of magnitude less than the morphological change that occurs in response to SLR. Moreover, the difference between the gravel and sand "primed" island morphology, with the former possessing a considerably steeper beachface and a higher crest elevation than the latter, is representative of natural coral reef islands (Kench et al., 2009, 2017; Figure S2).
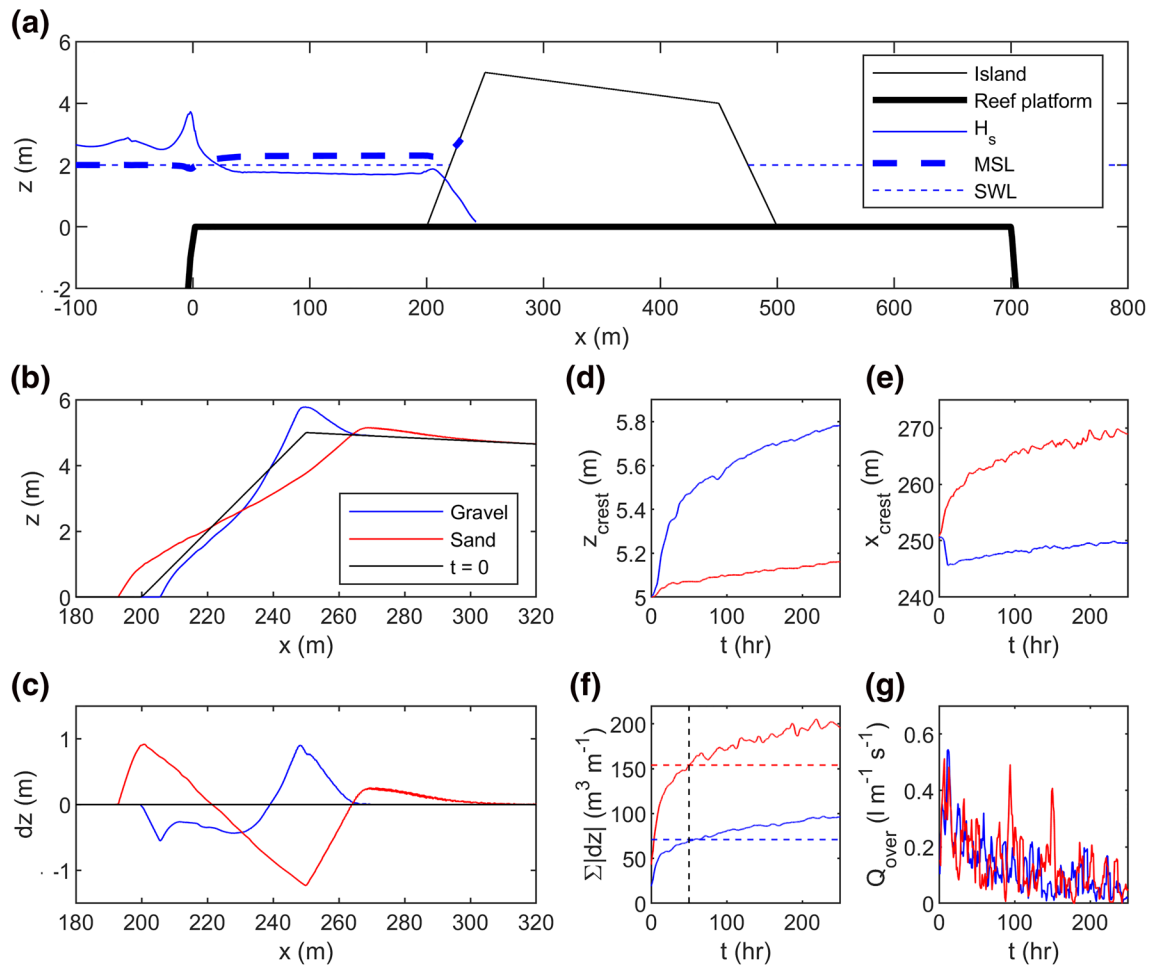
Figure 2. XBeach-G model results for 250-h simulation with constant wave forcing of $H_0 = 3$ m, $T_p = 9.9$ s and $h_{reef} = 2$ m, for gravel ($D_{50} = 14$ mm, $K = 0.005$ m s^{-1}) and sand ($D_{50} = 1$ mm, $K = 0$ m s^{-1}) island. (a) Model set-up with cross-shore variation in significant wave height H_s, wave set-up MSL and the tide level SWL. (b) Island morphology z and (c) morphological change dz after 250-h of wave action. Time series of (d) island crest elevation z_{crest}, (e) island crest position x_{crest}, (f) cumulative gross morphological change $\Sigma|dz|$ and (g) overwash discharge Q_{over} across the island crest. The horizontal dashed lines in (d) represents 75% of the total $\Sigma|dz|$ over the 250-h simulation, which occurred for both the gravel and sand simulation around $t = 50$ h (vertical dashed line). The time series were smoothed using a 5-h moving window.

2.5. Modeling Impact of Sea-Level Rise (Test C)

Using a processed-based model operating in real-time, such as XBeach-G, to model long-term coastal evolution as a result of SLR is potentially problematic and, at least, challenging (e.g., a 100-h morphodynamic simulation takes 100 h computing time on a 4-core Windows machine). An "input-filtering" approach was used here that assumes that whole-island change is only accomplished by extreme and infrequent wave conditions acting at high tide (cf., Masselink et al., 2020). Specifically, the rate of SLR was linked to hours of extreme wave action ($H_0 = 3$ m) operating at high tide ($h_{reef} = 2$ m at the start of the simulation). The island response to 1-m SLR was explored for three variations in total duration of extreme wave action occurring during the SLR period: 50, 100 and 200 h, representing 0.02, 0.01, and 0.005 m h^{-1} rate of SLR per hour of extreme wave conditions, respectively (**Test C**; Table S1). Assuming such conditions occur 1 h per year on average, the three rates represent annual SLR rates of 0.02, 0.01, and 0.005 m year^{-1}, respectively (i.e., 1-m SLR occurring in 50, 100, or 200 years, respectively). Alternatively, the three rates represent a variation in the number of hours of extreme waves per year for a given annual SLR rate, for example, 0.5, 1 and 2 h of extreme waves per year for a constant annual SLR rate of 0.01 m year^{-1}. As such, the approach is decoupled from SLR rate projections and instead describes the relationship between the speed at which sea level is rising and the available time to build up the island crest in response. This event-based modeling approach

does not fully describe coral reef island evolution over long time scales; however, the approach offers an experimental platform with which to consider the role of a range of important factors in coral reef island response to SLR, including sediment size, reef platform growth and wave height variability.

2.6. Accounting for Reef Platform Growth (Tests D and E)

After the 1-m SLR simulations, the response of gravel and sand islands to 2.5 m of SLR at a rate of 0.01 m h^{-1} of extreme waves was simulated with and without reef growth (**Test D**; Table S1). For the model simulations with reef growth, the entire reef structure (including reef platform) accretes at the same rate as SLR, but lagged behind by 1 h (i.e., 0.01 m). A "keep-up" scenario of reef grow is thus assumed and this will be contrasted by a "no-growth" scenario, with both representing end-members of a spectrum of reef growth behavior. When first accounting for reef growth, only that part of the reef platform not covered by sediment was allowed to grow, but island retreat due to roll-over resulted in the development of an unrealistically deep (>1 m) "moat" in front of the retreating island. In reality, such moat would be filled with sediment, but this does not happen according to the model. Instead, therefore, in the subsequent simulations with reef growth, the entire reef platform was allowed to grow with SLR, even underneath the island, but without modifying the elevation of the island. This approach does effectively lock up island sediment below the level of the reef platform and limits the amount of sediment available for remobilization and reworking during island retreat, but is necessary to avoid a 2.5-m deep and very narrow (several m's) moat in front of the retreating sand island at the end of the simulation (this is not an issue on the gravel island).

To investigate in detail the hydrodynamic conditions during the reef growth simulations, hourly averaged hydrodynamics were output for every 10 h of the 2.5-m SLR simulations (i.e., $t = 0, 10, 20, 30, ...$ h, or SLR $= 0, 0.1, 0.2, 0.3, ...$ m). For these model runs (**Test E**; Table S1), exactly the same hourly wave forcing was used throughout ($H_0 = 3$ m, $T_p = 9.9$ s), but four different morphological boundary conditions were used: (1) unmodified "primed" island morphology with static reef platform ($-M-RG$); (2) unmodified "primed" island morphology with reef platform growth ($-M+RG$); (3) modeled island morphology with static reef platform ($+M-RG$); and (4) modeled island morphology with reef platform growth ($+M+RG$). Regardless of the status of the reef platform, any sediment on the platform surface is mobile. In these simulations, the wave setup η, significant wave height H_s and incoming infragravity significant wave height $H_{s,inf,in}$ (computed using Guza & Thornton, 1985) at the toe of the beach (at $x = 190$ m), and the overwash discharge Q_{over} across the island crest were extracted from the modeled data.

2.7. Investigating Impact of Wave Height Variability (Tests F and G)

To start exploring the role of wave height variability on island response, the gravel and sand island morphology attained after 200 h of SLR with reef growth was exposed to a large number of 1-h simulations with H_0 increasing from 1 m to 5 m in 0.1-m steps and a sea level at 2.5 m, that is, 0.5 m higher than corresponding to $t = 200$ h (**Test F**; Table S1). The wave period was kept constant during all simulations to limit the amount of forcing and controlling factors; it is acknowledged that simulations with longer wave periods would have resulted in higher wave runup, larger overwash discharge and more extensive morphological change, for the same water level and wave height.

In the final set of simulations, island response to a 2.5-m SLR at a rate of 0.01 m h^{-1}, and accounting for reef growth, was modeled, but this time with variable wave conditions (**Test G**; Table S1). Forcing wave conditions were randomly selected from a triangular H_0 distribution with maximum probability for $H_0 = 2$ m and zero probability for $H_0 = 5$ m. The resulting 250-h time series of H_0 was characterized by a rms value of 3.1 m, thus representing only a slightly higher wave energy level than during the previous simulations with a constant wave height of $H_0 = 3$ m.

3. Results

3.1. Role of Rate of Sea-Level Rise on Island Response

The modeled evolution of the gravel and sand reef island in response to a 1-m increase in sea level from +2.0 to +3.0 m for the three different rates of SLR (**Test C**; Table S1) is shown in Figure 3. During all simulations,
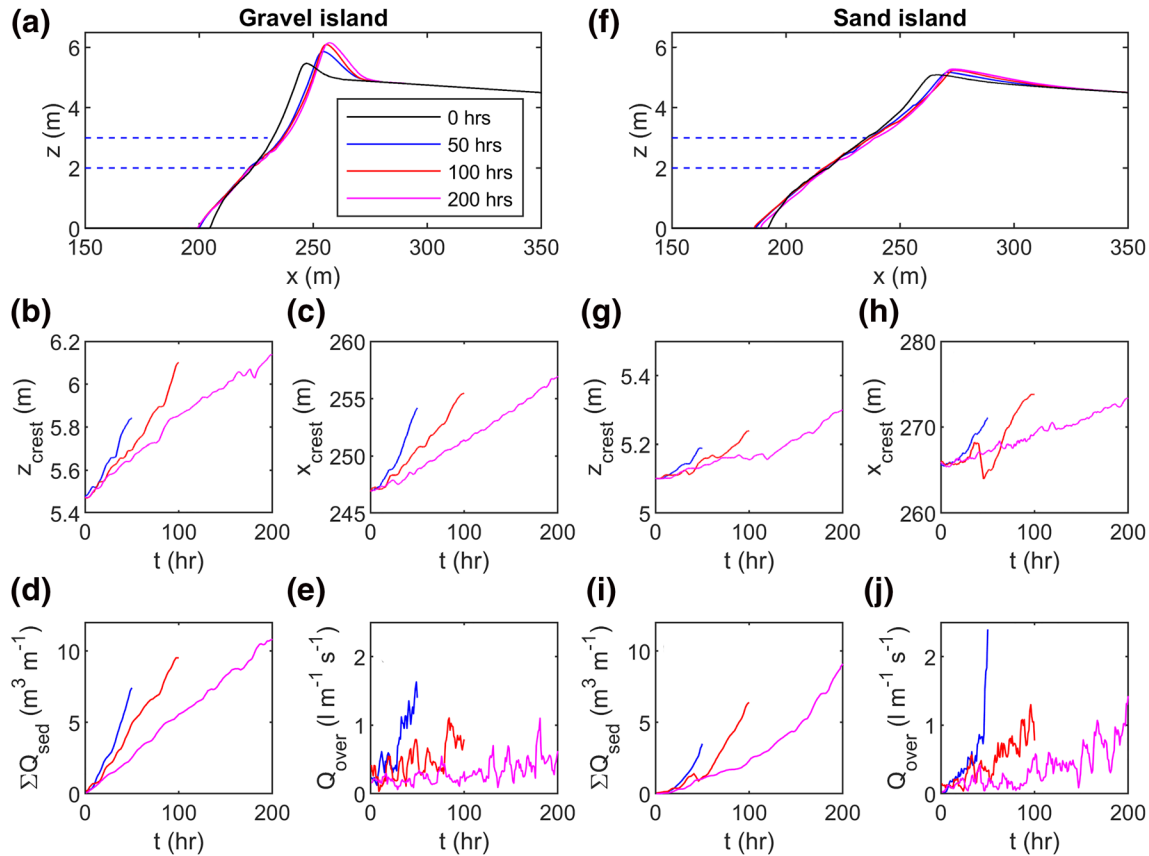
Figure 3. Modeled evolution of the gravel (left panels; a–e) and sand (right panels; f–j) reef island during a 1-m SLR (from $h = 2$ m to 3 m) with rates of SLR of 0.02, 0.01, and 0.005 m per 1 h of wave action with constant wave forcing of $H_0 = 3$ m, $T_p = 9.9$ s. (a and f) Island morphology at the start and end of model simulation, and time series of (b and g) island crest elevation z_{crest}, (c and h) island crest position x_{crest}, (d and i) cumulative sediment transport ΣQ_{sed} across the island crest and (e and j) overwash discharge Q_{over} across the island crest. Note the different y-axis scales for (b and g), and (c and h). The time series were smoothed using a 5-h moving window.

the island demonstrates roll-over behavior (Figure 3a and 3f), but the gravel island accretes and retreats more ($\Delta z_{crest} = 0.4$–0.7 m; $\Delta x_{crest} = 7$–10 m; Figure 3b and 3c) than the sand island ($\Delta z_{crest} = 0.1$–0.3 m; $\Delta x_{crest} = 5$–7 m; Figure 3g and 3h). The cumulative onshore sediment transport ΣQ_{sed} across the island crest is also larger for the gravel island ($\Sigma Q_{sed} = 7$–11 m^3 m^{-1}; Figure 3d) than the sand island ($\Sigma Q_{sed} = 3$–9 m^3 m^{-1}; Figure 3i). Offshore sediment transport also occurs, but is very limited with only a small amount of deposition at the toe of the island in both cases. The island crest accretes in all simulations, but the amount of freeboard (z_{crest}−SWL, where SWL denotes still water level) reduces throughout the simulation, especially for the sand island and for the fastest rate of SLR. This reduction in freeboard results in increased overwash discharge across the island crest during the simulations, but less so for the gravel island ($Q_{over} = 0.5$–1.5 l m^{-1} s^{-1}; Figure 3e) than the sand island ($Q_{over} = 1$–2.4 l m^{-1} s^{-1}; Figure 3j), and increasing with rate of SLR. The fluctuations in Q_{over} values, despite applying a 5-h moving average, occur because the hourly wave forcing varies stochastically as a new wave signal is generated at the start of each hour. There is less difference between the simulations with 100 and 200 h of wave action, than between those with 50 and 100 h of wave action, especially for the gravel island; therefore, and for reasons of expediency, a rate of SLR of 0.01 m h^{-1} of wave action was used in the remaining simulations.

3.2. Role of Reef Growth on Island Response to Sea-Level Rise

A 2.5-m SLR rising at 0.01 m h^{-1} of wave action was used to investigate the role of reef growth on gravel and sand island response (**Test D**; Table S1). Animations of the island response for the gravel and sand islands with a static reef are visualized in Movies S1 and S2. For the first 1.5 m of SLR from +2.0 to +3.5 m
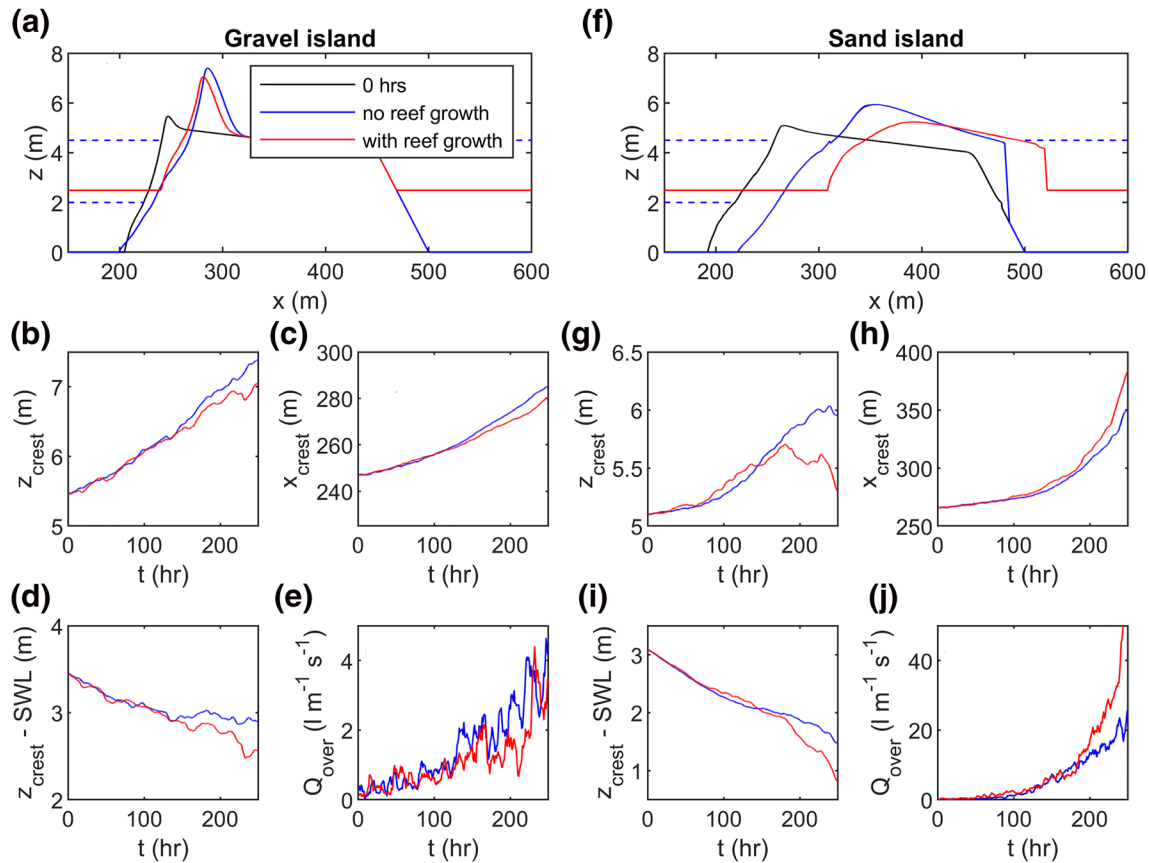
Figure 4. Modeled evolution of the gravel (left panels; a–e) and sand (right panels; f–j) reef island during a 2.5-m SLR with (blue lines; +RG) and without (red lines; −RG) reef growth keeping pace with rising sea level, and with constant wave forcing of $H_0 = 3$ m and $T_p = 9.9$ s. (a and f) Island morphology at the start and end of model simulation, and time series of (b and g) island crest elevation z_{crest}, (c and h) island crest position x_{crest}, (d and i) freeboard z_{crest}−SWL and (e and j) overwash discharge Q_{over} across the island crest. Note the different y-axis scales for the gravel (b–e) and sand (g–j) island. The time series were smoothed using a 5-h moving window.

($t = 150$ h), there was no significant difference in island evolution or overwash discharge between the simulations with and without reef growth (Figure 4). Both gravel and sand island accreted and retreated, but the gravel island accreted more ($\Delta z_{crest} = 0.8$ m; Figure 4b) than the sand island ($\Delta z_{crest} = 0.4$ m; Figure 4g), and the sand island underwent more retreat ($\Delta x_{crest} = 20$ m; Figure 4h) than the gravel island ($\Delta x_{crest} = 10$ m; Figure 4c). For both islands, the amount of SLR exceeded the change in z_{crest}; therefore, the amount of freeboard (z_{crest}−SWL) decreased, and this resulted in an increase of the overwash discharge Q_{over} during the simulations (Figure 4e and 4j).

During the last 100 h of the simulations, when sea level increased from +3.5 to +4.5 m, the gravel island without reef growth continued to accrete and retreat, maintaining a freeboard of 3 m with Q_{over} increasing from 2 to 5 l m^{-1} s^{-1} (Figure 4d and 4e). With reef growth, the gravel island also continued to accrete, but slightly less, attaining a freeboard of 2.5 m at the end of the simulation. Over the same period, the sand island without reef growth also continued to accrete and retreat, albeit at reduced and increased rate, respectively, and with freeboard reducing to 1.5 m and Q_{over} increasing from 5 to 25 l m^{-1} s^{-1} (Figure 4i and 4j). With reef growth, the sand island started to fail after 150 h, and by the end of the simulation only 0.5 m freeboard remained with $Q_{over} > 50$ l m^{-1} s^{-1}. The rate of retreat of the sandy island during the first 1 m SLR is relatively limited (<0.1 h^{-1}), but then rapidly accelerates to almost 1 m h^{-1} over the remainder of the simulation (Figure 4h).

It is of interest to relate the mean overwash discharge across Q_{over} the island crest to the sediment transport rate Q_{sed} across the island crest as one would expect a strong correlation between these two parameters. Hourly values of Q_{over} (in m^3 m^{-1} h^{-1}) and Q_{sed} (in m^3 m^{-1} h^{-1}) were extracted from the 250-h simulation
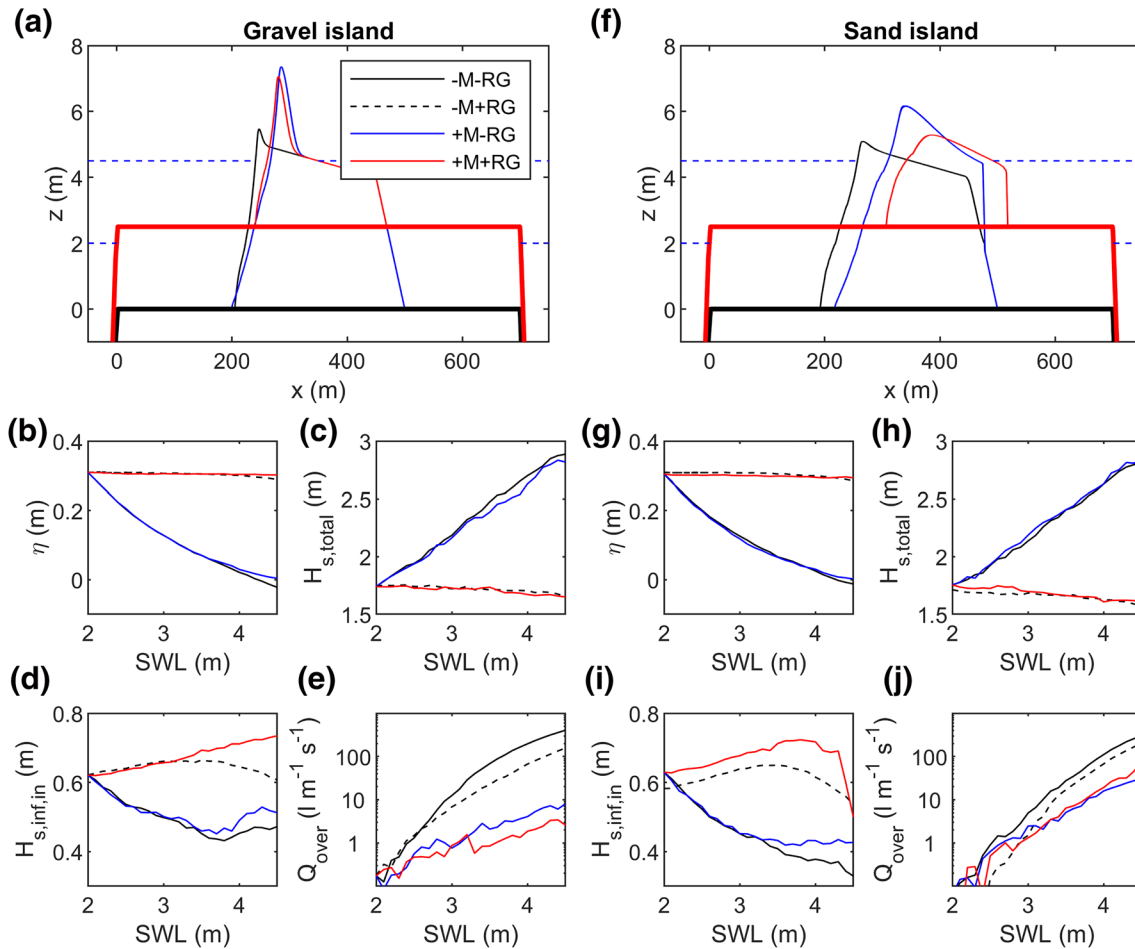
Figure 5. Modeled evolution and associated hydrodynamics of the gravel (left panels; a–e) and sand (right panels; f–j) reef island during a 2.5-m SLR with (+RG) and without (−RG) reef growth keeping pace with rising sea level, and with constant wave forcing of $H_0 = 3$ m, $T_p = 9.9$ s. (a and f) Island morphology at the start and end of model simulation, and time series of (b, g) wave setup η, (c and i) significant wave height H_s, (d and i) incoming infragravity significant wave height $H_{s,inf,in}$ and (e, j) overwash discharge Q_{over} across the island crest. The time series represent hourly averages for every 10 h of the 250-h simulation, and on the x-axis the SWL plotted rather than the time (SWL = 0 m represents level of the reef platform at start of simulation). Bold lines represent reef platform. The different runs represent: +M = evolving island; −M = unmodified island; +RG = with reef growth; and −RG = without reef growth.

with a 2.5-m SLR without reef growth and subjected to simply linear regression, resulting in $Q_{sed} = 0.078\ Q_{over}$ ($r^2 = 0.98$) for the gravel island and $Q_{sed} = 0.048 Q_{over}$ ($r^2 = 0.97$) for the sand island (Figure S3). This implies, that, for the same average overwash discharge Q_{over} across the crest, the gravel sediment transport rate is 60% greater than that of sand.

3.3. Hydrodynamics During Sea-Level Rise

The results indicate that, overall, reef growth does not appear to offset the physical impacts of SLR and make the reef islands more resilient. This result is somewhat surprising as it challenges prevailing insights on the importance of reef structure in affording some protection to island shorelines (Ferrario et al., 2014). Consequently, this result is further investigated through consideration of the hydrodynamics during the simulations (**Test E**; Table S1). Wave conditions at the toe of the beach for the simulations with static reef platform (−RG), regardless of whether the island morphology is constant (−M) or modeled (+M), are very similar and vary in a consistent manner with increasing sea level in line with Figure S1 (solid lines in 5b, 5e, 5g, 5h, and 5i). Wave conditions at the toe of the beach remain relatively constant if the reef platform keeps pace with SLR (dashed lines in Figures 5b–5e, 5g, 5h, and 5i). As expected, the beach morphology

has limited influence on the wave conditions across the reef platform. The overwash discharge across the island crest Q_{over} increases with SLR for all simulations (Figures 5f and 5j). For the unmodified gravel and sand island, $Q_{over} > 10\,l\,m^{-1}\,s^{-1}$ after 1-m SLR (SWL = 3 m), but Q_{over} does not exceed $1\,l\,m^{-1}\,s^{-1}$ if the reef platform keeps pace with SLR (+RG). This is especially apparent for the gravel island with the difference between reef growth and no growth increasing with SLR. For an evolving island, Q_{over} is much smaller than for the unmodified island, at least by up to one order of magnitude by the end of the simulation; however, the Q_{over} values with and without reef growth are very similar. The beach morphology has thus significant influence on the overwash characteristics.

If the morphological response of the island to SLR is ignored, then reef growth significantly reduces overwash discharge and coastal flooding, because the shallower water depths across the reef enhance wave energy dissipation and reduce wave runup, whilst at the same time maintaining wave set-up and infragravity wave action (cf., solid and black dashed lines in Figure 5). In that case, platform growth contributes positively to island resilience and helps mitigate the physical impacts of SLR. For an evolving island, however, the overwash discharge, and therefore the extent of coastal flooding and island inundation, does not depend greatly on whether the reef platform grows or not (cf., solid red and blue lines in Figures 5e and 5j). This can be explained by considering that, according to the numerical model, the island elevation adjusts to SLR such that z_{crest} matches more or less the maximum runup height $R_{2\%}$. Smaller h_{reef} values for a reef that keeps up with SLR therefore result in lower islands. The failure of the sandy island with reef growth (rapid reduction of freeboard during SLR) compared to the one without reef growth at the end of the simulation is puzzling. It is suggested that the higher wave setup η and incoming infragravity significant wave height $H_{s,inf,in}$ in the former case is less conducive to island maintenance than the higher significant wave height H_s in the latter case.

3.4. Dependence of Island Response to Wave Height

So far, only a single wave condition ($H_0 = 3$ m) has been used for the morphodynamic SLR simulations and this wave condition was selected on the basis of the wave runup it generates on the initial island morphology (cf., Figure 2). More energetic conditions are considered to be too infrequent to play a role in the elevation of the island and less energetic conditions do not reach the crest and can therefore not modify the top of the island. However, as island freeboard decreases, e.g., by the end of the 2.5-m SLR simulation of the sand island, less energetic wave conditions ($H_0 < 3$ m) should become increasingly able to reach the island crest and contribute positively to island maintenance. Similarly, more energetic wave conditions ($H_0 > 3$ m) should become increasingly destructive due to the larger overwash discharge. To illustrate such shift in wave height thresholds between "constructive" and "destructive" wave conditions (increase and decrease in island elevation, respectively), XBeach models were set-up using the gravel and sand island morphology that developed after 2-m SLR accounting for reef growth (i.e., morphology developed at $t = 200$ h in **Test D**; Table S1), and offshore wave conditions ranging from of $H_0 = 1$ m to 5 m in 0.1-m steps (**Test F**; Table S1). A sea level of 4.5 m, representing a SLR of 2.5 m, was used to deliberately reduce the island freeboard by 0.5 m to bring out the role of wave height in island development. The change in island morphology (dz_{crest} and dx_{crest}) and overwash characteristics (mean overwash depth h_{crest} and discharge Q_{over} across the island crest) for each 1-h simulation was computed and plotted as a function of H_0 (Figure 6).

The results for both "underfit" islands, that is, islands with significantly reduced freeboard compared to the start of the simulation, indicate that raising of the island crest ($dz_{crest} > 0$) occurs for all wave conditions characterized by $H_0 < 3$ m, while the crest location remains relatively constant ($dx_{crest} < 3$ m; Figures 6b and 6c). Such wave conditions correspond to hydrodynamic thresholds of $dh_{crest} = 0.01$ m and $Q_{over} = 5\,l\,m^{-1}\,s^{-1}$ for the gravel island, and $dh_{crest} = 0.03$ m and $Q_{over} = 20\,l\,m^{-1}\,s^{-1}$ for the sand island (Figures 6d and 6e). For $H_0 > 3$ m, the island crest is lowered and retreats with increasing H_0. Subjecting the gravel island to $H_0 = 5$ m for only 1 h, results in a decrease in crest height of 1 m and crest retreat of 10 m, and is associated with $h_{crest} = 0.08$ m and $Q_{over} = 150\,l\,m^{-1}\,s^{-1}$. For the sand island, a decrease in crest height of 0.5 m and crest retreat of 20 m is associated with $h_{crest} = 0.15$ m and $Q_{over} = 350\,l\,m^{-1}\,s^{-1}$. It thus appears that the crest of the gravel barrier is morphologically more responsive to destructive wave conditions than the crest of the sand island, despite the smaller overwash depths and discharge; but, on the sand island, due to its impermeable
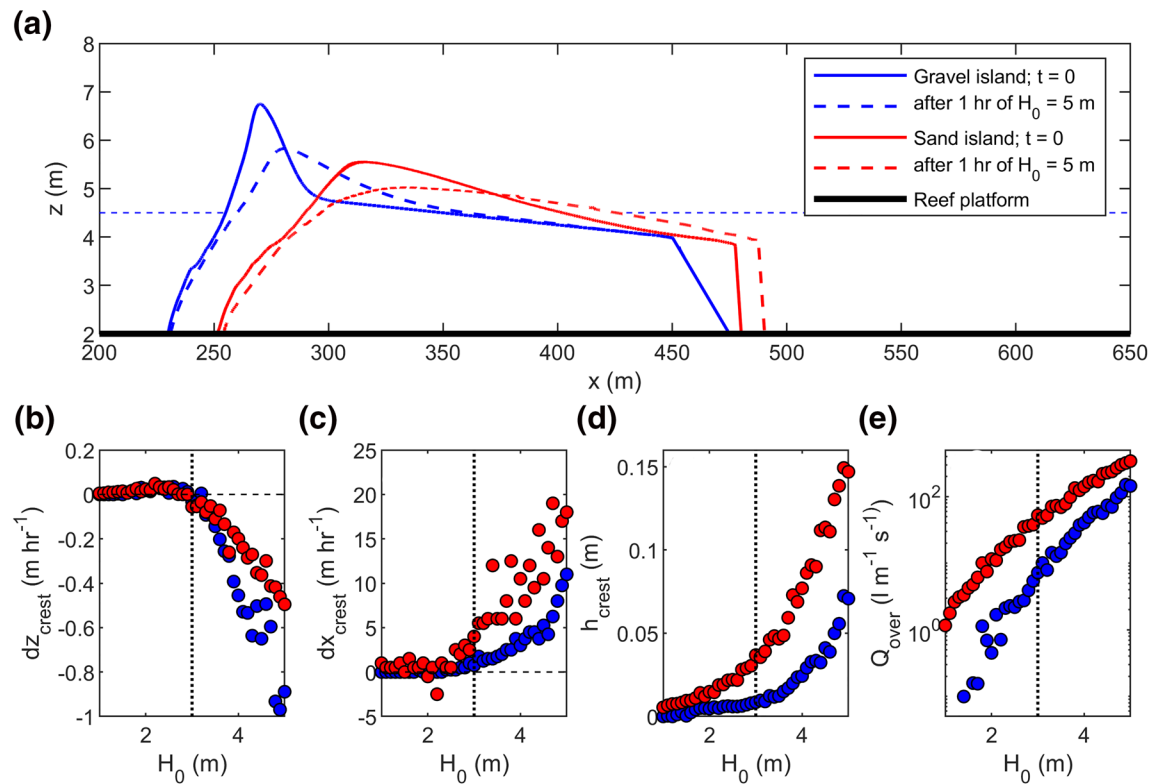
Figure 6. (a) Gravel and sand island morphology after 2 m SLR at $t = 200$ h during test D, but with sea level and reef platform representing a SLR of 2.5 m, which was subjected to offshore wave heights increasing from $H_0 = 1$ m to 5 m in 0.1-m steps for 1 h for each wave conditions. Dashed lines show island morphology after 1 h of $H_0 = 5$ m. Lower panels show the relationship, for gravel (blue circles) and sand (red circles) island, between offshore wave height H_0 and: (b) change in crest elevation dz_{crest}; (c) change in crest position dx_{crest}; (d) average water depth h_{crest} across island crest; and (e) overwash discharge Q_{over} across island crest. The vertical dotted line at $H_0 = 3$ m represents the approximate wave height threshold between island crest building and destruction. Mean h_{crest} is computed over the whole simulation, including zeros when dry.

nature in the model, overwash occurs across the entire island resulting in washover deposits behind the barrier (i.e., complete washover; Figure 6a). Animations of the overwash characteristics at either side of the $H_0 = 3$ m threshold are visualized in Movies S3 and S4.

3.5. Considering the Full Energetic Part of the Wave Climate ($H_0 > 2$ m)

In the final set of simulations, gravel and sand island response to a 2.5-m SLR at a rate of 0.01 m h^{-1}, and accounting for reef growth, was modeled, with variable wave conditions ($H_0 = 2$–5 m; **Test G**; Table S1). The gravel island continues to accrete and retreat during SLR, whilst retaining freeboard (Figures 7a and 7b), and the final morphology is actually quite similar to the simulation with constant wave conditions (cf., Figures 6a and 6b). In contrast, the sand island initially accretes modestly and retreats up to $t = 150$ h (1.5-m SLR), but then rapidly looses freeboard and shows "run-away" migration, becoming permanently submerged after $t = 200$ h and with all sediment transferred into the lagoon by the end of the simulation (Figures 7e and 7f). In the simulations with constant wave conditions and reef growth, the sand island also starts to "fail" around $t = 150$ h (cf., Figures 7f and 7g), but not as spectacular as with variable wave conditions. The disparate trajectories of the gravel and sand island are directly linked to the overwash discharges across the island crest with $Q_{over} < 20$ l m^{-1} s^{-1} throughout the simulation for the gravel island and $Q_{over} > 100$ l m^{-1} s^{-1} after $t = 150$ h for the sand island (Figures 7c and 7g).

During the run with variable wave conditions, z_{crest} increases and decreases depending on the energy level of the wave conditions driving the amount of overwash. To explore this relation in more depth, Figures 7d and 7h relates Q_{over} to the hourly change in island crest elevation dz_{crest}, where each data point represents
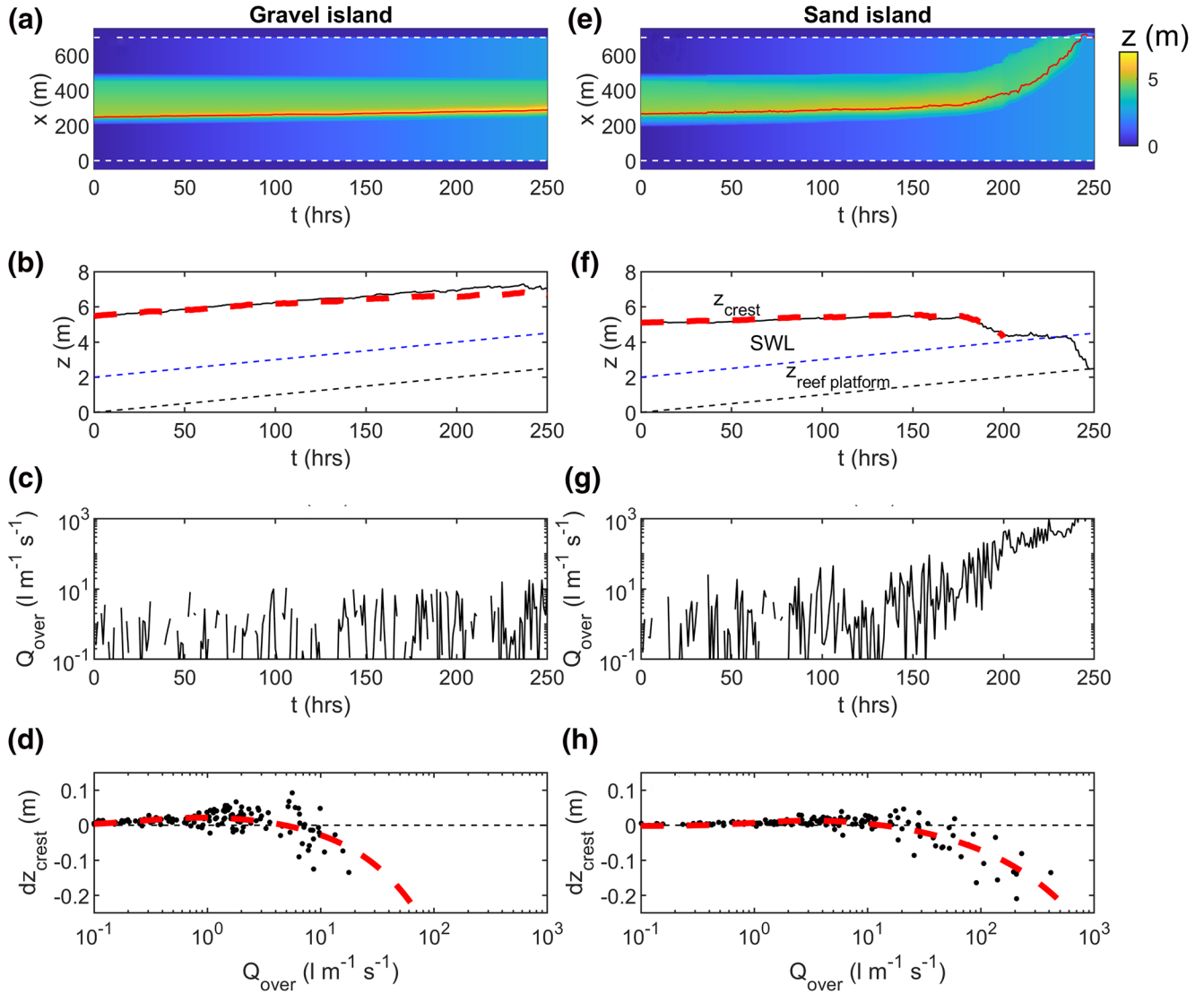
Figure 7. Modeled evolution of the gravel (left panels; a–d) and sand (right panels; e–h) reef island during a 2.5-m SLR with reef growth keeping pace with rising sea level, and with variable wave forcing of $H_0 = 2$–5 m and $T_p = 9.9$ s. (a and e) Evolution of island morphology with color representing elevation, red line indicating position of island crest and horizontal white dashed lines representing edge of reef platform. (b and f) Time series of island crest elevation z_{crest}, still water level SWL and elevation of reef platform z_{reef} platform; red dashed line represents z_{crest} predicted using the fitted line to the data in (d and h). (c and g) Time series of overwash discharge across the island crest Q_{over} with gaps in the time series indicating wave runup did not reach the island crest (i.e., $Q_{over} = 0$). (d and h) Scatter plots of Q_{over} versus hourly change in island crest elevation dzcrest with the red dashed line representing the best fit line.

1 hour of variable forcing ($H_0 = 2$–5 m). A similar plot was presented earlier where dz_{crest} was related to H_0 using results of **test F** (cf., Figure 6). For both the gravel and sand island, the model data show positive dz_{crest} values for relatively small values of Q_{over}, and negative dz_{crest} values for relatively large values of Q_{over}, with a threshold value for Q_{over} of 5 and 20 l m^{-1} s^{-1} for gravel and sand island, respectively. An equation was fitted to the data of the form:

$$d_{z,crest} = \left[a_1 \tan h \left(b_1 \log Q_{over} + c_1 \right) + a_1 \right] + \left[a_2 \exp \left(b_2 \log Q_{over} + c_2 \right) \right] (1)$$

where [a_1, a_2, b_1, b_2, c_1, c_2] are fitting coefficients (gravel = [1/50, −1/94, 1.7, 1.7, 0.85, 0.15 with $r^2 = 0.36$]; sand = [1/50, −1/70, 1.6, 1.2, −0.15, −0.35 with $r^2 = 0.69$]). The first and second term in the Equation 1 represent the crest accretion ($d_{z,crest} > 0$) and crest erosion ($d_{z,crest} < 0$) part of the data, respectively. Despite considerable scatter, application of Equation 1 to predict the evolution of $d_{z,crest}$ as a function of the hourly

mean overwash discharge Q_{over} matches the numerical model output quite well (Figure 7b for gravel island; Figure 7f for sand island).

4. Discussion

Masselink et al. (2020) introduced the numerical model approach used in the present paper and demonstrated that coral reef islands composed of gravel have the potential to vertically accrete in response to a 1-m SLR to retain freeboard, confirming physical modeling (Tuck, Ford, et al., 2019; Tuck, Kench, et al., 2019). This ability of islands to vertically accrete under energetic wave and/or water level forcing has also been demonstrated by field observations (Hoeke et al., 2013; Kench & Beetham, 2019; Kench et al., 2006). The model results of Masselink et al. (2020) also showed that the maximum increase in island elevation was associated with a mean crest discharge of 0.01–0.02 $m^3\,m^{-1}\,s^{-1}$ (10–20 $l\,m^{-1}\,s^{-1}$), with higher discharge magnitudes resulting in crest lowering. This paper confirms and significantly extends these results; specifically, we have now also considered the response of sand islands, extended the magnitude of SLR to 2.5 m, evaluated the role of future reef growth on island response, and explored the importance of wave height variability. We stress that our simulations purposely adopted higher magnitudes of SLR (representing >100-years time horizon) and wave energies to purposely evaluate morphological behaviors and critical thresholds that denote changes in physical response to boundary process conditions.

4.1. Limitations

Despite the sophistication of the processed-based model used here, accounting for wave-resolving hydrodynamics and swash-groundwater interactions, there are many factors that also play an important role in driving and/or controlling reef island response to SLR that have not been considered. These include: the influence of temporally varying rates of SLR which may afford differential relaxation periods for morphological response; the effect of width, shape and roughness of the reef platform on wave transformation processes (Pearson et al., 2017; Quataert et al., 2015); the potentially stabilizing role of island vegetation (Duvat & Pillet, 2017); the presence of island infrastructure providing obstructions and/or conduits for overwash on inhabited islands (Duvat & Magnan, 2019); and the potentially stabilizing role of sediment supply to the island (gravel and sand) from the reef system (Dawson & Smithers, 2014; Gischler & Lomando, 1999; Kayanne et al., 2016; Perry et al., 2011).

It is also relevant to point out that only the gravel island model settings have been validated with the small-scale physical experiment reported in Tuck, Kench, et al. (2019) and that, to date, there has been no validation of the sand island model. Barrier island studies could serve as an analogue for the sand island model, but only the phase-averaged version of the XBeach model has been implemented in these settings (e.g., McCall, et al, 2010; Van der Lugt et al., 2019). Additionally, identical starting morphology and position for the gravel and sand island on the reef platform is not realistic, as gravel islands tend to be higher and are generally located at more exposed locations on the platform than sand islands (Stoddart & Steers, 1977). In the simulations with a "keep-up" reef growth scenario, the lower part of the island below the reef platform level is immobilized, effectively removing sediment from the circulation. For a retreating island and onshore sediment transport, this sediment would normally have been supplied to the upper part of the island, reducing the rate of island retreat. This removal of sediment from the island sediment budget may have affected the response of the sand and gravel island to SLR disproportionally. Specifically, the sand island retreated significantly further than the gravel island (cf. Figures 4a and 4f) and this difference may have been enhanced by the lower beach sediment not being part of the sediment transport system. A final limitation is the simplification of island and reef morphology to a one-dimensional (1D) profile that does not account for wave refraction and alongshore sediment transport; however, Tuck, Ford, et al. (2019) demonstrated that the central island profile in their two-dimensional (2D) wave basin experiment responded very similar to SLR than the island profile in their 1D wave flume experiment.

Nevertheless, despite the simplified representation of the reef-island topography and the exclusion of several important factor and processes in the modeling approach, the key results of this modeling study are insightful and merit further discussion.

4.2. Gravel Versus Sand Island Response

Both gravel and sand islands show vertical accretion in response to SLR (cf., Masselink et al., 2020), but the model results suggest that the gravel island is better able to retain freeboard than the sand island, and could be considered more resilient to SLR. This is evident by the end of the 2.5-m SLR simulation, when, if reef growth is ignored, the elevation of the gravel island crest level increased by almost 2 m, while the sand island crest was only raised by c. 1 m (cf., Figure 4). If reef growth is considered, the difference between gravel and sand island response to a 2.5-m SLR is even more pronounced: the gravel island accreted 1.5 m, whereas the sand island was almost destroyed by the end of the simulation (cf., Figure 4). If a variable wave climate is used and reef growth is considered, the sand island is completely destroyed by the end of the 2.5-m SLR simulation, while the gravel island retains more than 1.5 m freeboard by the end of the simulation (Figure 7).

The difference in response to SLR between gravel and sand islands can be explained, in part, by wave runup and overwash characteristics, and also overwash infiltration losses, as they were modeled in the simulations. The lower elevation of the modeled sand island is directly related to the fact that sandy beaches have gentler beach gradients than gravel beaches (Bujan et al., 2019). A gentler beach gradient reduces wave runup height (Poate et al., 2016; Stockdon et al., 2006) and the ability of the waves to vertically construct the island as island crest level is "tuned" by the maximum runup elevation. The lower elevation and less resilient behavior of the sand island is also attributed to the larger transportability and smaller hydraulic conductivity of sand-sized material compared to gravel. On the modeled sand island, all overwash flowed down the backslope of the island to the lagoon. As the back-slope is relatively constant, high flow velocities and transport rates are maintained, limiting sediment deposition around the island crest and causing accretion to occur across the entire width of the island and in the form of washover deposits, as also documented in field observations (e.g., Leatherman, 1979; Matias et al., 2016; McCall et al., 2010). In contrast, the gravel material is more resistant to movement and has a high hydraulic permeability. Overwash water will be rapidly lost through infiltration after passing the island crest and this will result in localized sediment accretion around the crest location, without any water or sediment flowing across the back of the island (e.g., Matias et al., 2012).

The difference between sand and gravel fluxes is evident from, and can be expressed by, the amount of morphological change during the model simulations. It is well established that gravel is generally more resistant to transport than sand, but the beachface of the gravel island is steeper than that of the sandy island, driving more energetic onshore swash conditions and also affecting the overwash characteristics. On the gravel island, overwashes tend to be thinner, but with faster flows than on the sandy island. As a result, for the same overwash discharge, gravel sediment transport rates are significantly larger than for sand (Figure S1). This is evident during the 1-m SLR simulation, showing larger sediment fluxes with lower overwash discharges on the gravel island compared to that on the sand island (Figure 3). For the 2.5-m SLR simulations (Figures 4 and 5) and under more energetic forcing wave conditions (Figure 6), sand fluxes are substantially larger than gravel fluxes, but here the overwash discharge on the sand island is much larger than on the gravel island.

These are all relevant and very fundamental differences between gravel and sand islands, and they are likely to respond very differently to SLR. Another factor not considered in the modeling approach is the presence of island vegetation, which might be especially relevant for the sand islands which can be densely vegetated. Vegetation not only slows down the flows, but also acts to stabilize the surface of the island; both factors are expected to increase island resilience.

4.3. Role of Future Reef Growth

The influence of vertical reef platform growth on reef island hydrodynamics and island response to SLR is investigated here through modeling the two end-members on the reef growth spectrum: no-growth and keep-up growth. The viability of a future keep-up scenario may be justified by known rates of reef accretion of 10–20 mm y^{-1} over the past 1,000 years (Roff et al., 2015) and maximum measured rates of contemporary reef accretion (of up to 11.9 mm y^{-1}) that are comparable with rates of SLR under both RCP 4.5 and 8.5 scenarios (Perry et al., 2018; Van Woesik et al., 2018). However, these are maximum growth rates representing

forereefs with high-coral cover and environmental conditions optimal for growth. Growth rates on reef platforms are expected to be significantly lower and SLR is likely to result in a deepening of the reef platform; however, since no field data are available for contemporary reef platform growth rates, an end-member reef growth approach was adopted.

Model results suggest that, for an evolving island, reef growth has little influence on overwash discharge, coastal flooding and island inundation. In other words, reef growth does not seem to make the naturally evolving islands more resilient to SLR. This is a surprising finding and counter-intuitive given the protective role widely bestowed upon reef platforms. However, such assertions have previously been based on hydrodynamic modeling studies conducted for static and nonchanging island structures (Beetham et al., 2017; Pearson et al., 2017; Quataert et al., 2015), typical for densely populated islands. The difference between previous model studies and the current one arises because in the present morphodyamic modeling approach, the island adjusts morphologically to SLR such that z_{crest} matches more or less the maximum runup height $R_{2\%}$, with the latter largely a function of incident wave forcing H_0 and water depth across the reef platform h_{reef} (cf., Figure 1). In case of a progressively deepening reef platform during SLR (i.e., without reef growth), the increasingly energetic swash regime will drive higher wave runup, leading to a more elevated island crest. If the reef platform keeps pace with SLR (i.e., with platform growth), the swash regime remains relatively benign and, even though the island crest will still vertically accrete during SLR, z_{crest} will remain lower than in the case of a static reef platform elevation (cf., Figures 4a, 4b, 4f, and 4g). Conversely, if island adjustment is not included in the model, or not possible in reality due to topographic or anthropogenic constraints (e.g., seawall), reef platform growth does contribute positively to island resilience as suggested by previous hydrodynamic studies (Beetham et al., 2017; Pearson et al., 2017; Quataert et al., 2015). This occurs because the constant h_{reef} during SLR continues to dissipate incoming wave energy, limiting wave runup, overwash discharge and coastal flooding. Hydrodynamic and morphodynamic models can thus yield contradicting results.

4.4. Impact of Wave Height Variability

A single wave height value of $H_0 = 3$ m was used in most simulations and its choice was informed by exposing the idealized island morphology to a range of wave conditions and selecting the wave height that just overtopped the island crest. There are many coral reef islands, however, that experience either more (e.g., Marshall Islands; Storlazzi et al., 2018) or less (e.g., Maldives; Wadey et al., 2017) energetic wave conditions; therefore, the role of different wave conditions ($H_0 = 2$–5 m), including the occurrence of tropical cyclone waves every few years to decades, was considered in the final set of simulations, whilst also considering reef growth. The response of the gravel island to 2.5-m SLR with variable wave conditions was very similar to using constant wave conditions, but the sand island was completely eroded by the end of the simulation with variable wave conditions (cf., Figure 7). The most useful aspect of these simulations is that it exposes the reef island to hourly fluctuations in the overwash discharge Q_{over} that can be correlated to the hourly change in island crest elevation dz_{crest}. The gravel and sand island vertically accrete ($dz_{crest} > 0$) as long as $Q_{over} < 5 \, l \, m^{-1} \, s^{-1}$ and $< 20 \, l \, m^{-1} \, s^{-1}$, respectively.

There is considerable scatter in the Q_{over}–dz_{crest} plots based on the simulations with variable wave forcing (Figures 7d and 7h), but fitted lines explain a considerable amount of variability in the data. These fitted equations were implemented to provide an alternative means to model the evolution of the island crest elevation statistically by using only the hourly averaged Q_{over}. The results obtained from application of the statistical model show good agreement with the numerical model results (Figures 7b and 7f). This analysis perhaps points toward a way to model island evolution, at least the evolution of the island crest, taking into account the full wave climate and water level variability. Such an approach could involve: (1) using the BEWARE or a similar data set to predict overwash discharge across the crest as a function of reef-island topography (reef width, roughness, island elevation, and beach slope), water depth across the reef platform and wave conditions (height and period) (as per Figure 1); (2) use XBeach to create a data set to predict crest change from overwash discharge for different island geometries and sedimentologies; and (3) combine (1) and (2) into a simple model forced by a very large number of realizations of H_0, T_p and h_{reef} time series to predict the long-term evolution of the island crest elevation.

4.5. Implications

The results show that coral reef islands can vertically accrete via flooding and overwash if specific oceanographic and sedimentary conditions exist, and this notion should be taken into account when considering the future of these islands. In particular, our simulations that assume a finite sediment reservoir, high magnitude SLR and energetic wave conditions, present a worst-case set of constraints on island response. Consequently, results underscore considerable island resilience. In addition, anthropogenic activities that disrupt the natural sedimentary system, such as coastal defense works, will require careful consideration as, on the one hand they prevent flooding that can negatively impact infrastructure, freshwater availability, agriculture and terrestrial habitats, but on the other hand these measures also prevent the island from naturally adjusting through overwash deposition.

The findings also highlight that future trajectories of coral reef islands will also be influenced by coral reef ecology, specifically future reef platform accretion rates and reef sediment production/delivery to the reef islands. As shown in this study, adjustments in reef level will modify wave processes and interactions with an evolving shoreline. However, future reef growth trajectories still remain uncertain. Future SLR may outpace new reef flat accretion at many sites, resulting in an increase in water depth over coral reefs (Perry et al., 2018), although the exact magnitude is unclear. Our results show possible island responses in the absence of new inputs of detrital sediment. Intuitively, the addition of sediment should positively influence island physical response and resilience, though knowledge of the rates of sediment generation, the temporal variability in sediment generation and its delivery to islands are poorly constrained (Perry et al., 2012; Yates et al., 2017). While new supplies of sediment are necessarily reliant on a healthy reef state over decadal timescales, many reefs are subject to anthropogenic stresses that may reduce carbonate sediment production that is supplied to coral reef islands (Perry et al., 2012). Better constraining carbonate sediment production, sediment delivery from the coral reefs to the islands and how climate change and SLR may affect those processes (e.g., East et al., 2020; Storlazzi et al., 2011) are key to better forecasting how coral reef islands may evolve in the following decades (Winter et al., 2020).

5. Conclusions

A process-based numerical model was used to simulate the morphological response of gravel and sand coral reef islands to SLR and investigate the role of future reef growth on island response. The model results indicate that reef islands can evolve during SLR by accreting to maintain positive freeboard while retreating lagoonward by means of overwash. As long as the mean overwash discharge across the island crest remains below a certain threshold $O\,(10\,\mathrm{l\,m^{-1}\,s^{-1}})$, islands accrete vertically during SLR. A larger overwash discharge results in lowering of the island which can ultimately lead to island destruction under extreme forcing scenarios. Although the presence of a shallow reef platform in front of an island significantly reduces the wave energy incident at the island shoreline, due to wave breaking across the platform, model outputs show future reef growth does not increase the ability of islands to adjust to SLR on the medium-term (<50 years). This is because the maximum elevation of reef islands that keep pace with SLR, and thus maintain positive freeboard, is attuned to the maximum wave runup. Thus, islands fronted by a growing reef platform that keeps pace with SLR attain lower elevations than those without reef growth due to reduced wave energy at the shoreline, but will have a similar overwash regime. The model also indicates that, for the same oceanographic forcing, gravel islands build up higher than sand islands due to their steeper beachface gradient leading to higher runup. In conclusion, islands can grow vertically to keep up with SLR via flooding and overwash if specific forcing and sediment supply conditions are met, offering hope for uninhabited and sparely populated islands; however, on urbanized islands, mechanisms driving physical island response will negatively impact infrastructure and assets.

Data Availability Statement

As this study is solely based on numerical modeling, data were not used, nor created from this research. The numerical model setup and model results for the 2.5-m SLR for the sand and gravel island are available from https://doi.org/10.24382/bcbb-vc12.

References

Beetham, E., & Kench, P. S. (2018). A global tool for predicting future wave-driven flood trajectories on atoll islands. *Nature Communications*, *9*, 3997. https://doi.org/10.1038/s41467-018-06550-1

Beetham, E., Kench, P. S., & Popinet, S. (2017). Future reef growth can mitigate physical impacts of sea-level rise on atoll islands. *Earth's Future*, *5*, 1002–1014. https://doi.org/10.1002/2017EF000589

Bergillos, R. J., Masselink, G., & Ortega-Sánchez, M. (2017). Coupling cross-shore and longshore sediment transport to model storm response along a mixed sand-gravel coast under varying wave directions. *Coastal Engineering*, *129*, 93–104. https://doi.org/10.1016/j.coastaleng.2017.09.009

Brown, B. E., Dunne, R. P., Phongsuwan, N., & Somerfield, P. J. (2011). Increased sea level promotes coral cover on shallow reef flats in the Andaman Sea, eastern Indian Ocean. *Coral Reefs*, *30*, 867. https://doi.org/10.1007/s00338-011-0804-9

Bujan, N., Cox, R., & Masselink, G. (2019). From fine sand to boulders: examining the relationship between beach-face slope and sediment size. *Marine Geology*, *417*, 106012. https://doi.org/10.1016/j.margeo.2019.106012

Carruthers, E. A., Lane, D. P., Evans, R. L., Donnelly, J. P., & Ashton, A. D. (2013). Quantifying overwash flux in barrier systems: An example from Martha's Vineyard, Massachusetts, USA. *Marine Geology*, *343*, 15–28. https://doi.org/10.1016/j.margeo.2013.05.013

Cheriton, O., Storlazzi, C. D., & Rosenberger, K. (2016). Observations of wave transformation over a fringing coral reef and the importance of low-frequency waves and offshore water levels to runup, overwash, and coastal flooding. *Journal of Geophysical Research: Oceans*, *121*, 3121–3140. https://doi.org/10.1002/2015JC011231

Dawson, J. L., & Smithers, S. G. (2014). Carbonate sediment production, transport, and supply to A coral cay at Raine Reef, Northern Great Barrier Reef, Australia: A facies approach. *Journal of Sedimentary Research*, *84*, 1120–1138. http://dx.doi.org/10.2110/jsr.2014.84

Duvat, V. K. E., & Magnan, A. K. (2019). Rapid human-driven undermining of atoll island capacity to adjust to ocean climate-related pressures. *Scientific Reports*, *9*, 15129. https://doi.org/10.1038/s41598-019-51468-3

Duvat, V. K. E., & Pillet, V. (2017). Shoreline changes in reef islands of the Central Pacific: Takapoto Atoll, northern Tuamotu, French Polynesia. *Geomorphology*, *282*, 96–118. https://doi.org/10.1016/j.geomorph.2017.01.002

East, H. K., Perry, C. T., Beetham, E. P., Kench, P. S., & Liang, Y. (2020). Modelling reef hydrodynamics and sediment mobility under sea-level rise in atoll reef island systems. *Global and Planetary Change*, *192*, 103196. https://doi.org/10.1016/j.gloplacha.2020.103196

EurOtop, Van der Meer, J. W., Allsop, N. W. H., Bruce, T., De Rouck, J., Kortenhaus, A., Pullen, T. et al. (2018). *Manual on wave overtopping of sea defences and related structures*. An overtopping manual largely based on European research, but for worldwide application. Retrieved from www.overtopping-manual.com

Ferrario, F., Beck, M. W., Storlazzi, C. D., Micheli, F., Shepard, C. C., & Airoldi, L. (2014). The effectiveness of coral reefs for coastal hazard risk reduction and adaptation. *Nature Communications*, *5*, 3794. https://doi.org/10.1038/ncomms4794

Gischler, E., & Lomando, A. J. (1999). Recent sedimentary facies of isolated carbonate platforms, Belize-Yucatan system, Central America. *Journal of Sedimentary Research*, *69*, 747–763. https://doi.org/10.2110/jsr.69.747

Guza, R. T., & Thornton, E. B. (1985). Observations of surf beat. *Journal of Geophysical Research*, *90*, 3161–3172. https://doi.org/10.1029/JC090iC02p03161

Harter, C., & Figlus, J. (2017). Numerical modeling of the morphodynamic response of a low-lying barrier island beach and foredune system inundated during Hurricane Ike using XBeach and CSHORE. *Coastal Engineering*, *120*, 64–74. https://doi.org/10.1016/j.coastaleng.2016.11.005

Hoegh-Guldberg, O. (1999). Climate change, coral bleaching and the future of the world's coral reefs. *Marine and Freshwater Research*, *50*, 839–866. https://doi.org/10.1071/MF99078

Hoeke, R., McInnis, K. L., Kruger, J. C., McNaught, R. J., Hunter, J. R., & Smithers, S. G. (2013). Widespread inundation of Pacific islands triggered by distant-source wind-waves. *Global and Planetary Change*, *108*, 128–138. https://doi.org/10.1016/j.gloplacha.2013.06.006

Houser, C. (2013). Alongshore variation in the morphology of coastal dunes: Implications for storm response. *Geomorphology*, *199*, 48–61. http://dx.doi.org/10.1016/j.geomorph.2012.10.035

Hughes, T.P., Kerry, J. T., Álvarez-Noriega, M., Álvarez-Romero, J. G., Anderson, K. D., Baird, A. H., et al. (2017). Global warming and recurrent mass bleaching of corals. *Nature*, *543*, 373–377. https://doi.org/10.1038/nature21707

Kayanne, H., Aokei, K., Suzuki, T., Hongo, C., Yamano, H., Ied, Y., et al. (2016). Eco-geomorphic processes that maintain a small coral reef island: Ballast Island in the Ryukyu Islands, Japan. *Geomorphology*, *271*, 84–93. https://doi.org/10.1016/j.geomorph.2016.07.021

Kench, P. S., & Beetham, E. P. (2019), *Evidence of vertical building of reef islands through overwash and implications for island futures* (pp. 916–929). Paper presented at Proceedings Coastal Sediments'19, ASCE, Tampa, USA

Kench, P. S., Beetham, E., Bosserelle, C., Kruger, J., Pohler, S., Coco, G., & Ryan, E. (2017). Nearshore hydrodynamics, shoreline sediment fluxes and morphodynamics on a Pacific atoll Motu. *Marine Geology*, *389*, 17–31. https://doi.org/10.1016/j.margeo.2017.04.012

Kench, P. S., McLean, R. F., Brander, R. W., Nichol, S. L., Smithers, S. G., Ford, M. R., et al. (2006). Geological effects of tsunami on mid-ocean atoll islands: The Maldives before and after the Sumatran tsunami. *Geology*, *34*, 177–180. https://doi.org/10.1130/G21907.1

Kench, P. S., Parnell, K. E., & Brander, R. W. (2009). Monsoonally influenced circulation around coral reef islands and seasonal dynamics of reef island shorelines. *Marine Geology*, *266*, 91–108. https://doi.org/10.1016/j.margeo.2009.07.013

Lashley, C. H., Roelvink, D., van Dongeren, A., Buckley, M. L., & Lowe, R. J. (2018). Nonhydrostatic and surfbeat model predictions of extreme wave run-up in fringing reef environments. *Coastal Engineering*, *137*, 11–27. https://doi.org/10.1016/j.coastaleng.2018.03.007

Leatherman, S. P. (1979). Migration of assateague Island, Maryland, by inlet and overwash processes. *Geology*, *7*, 104–107. https://doi.org/10.1130/0091-7613(1979)7<104:MOAIMB>2.0.CO;2

Lindemer, C. A., Plant, N. G., Puleo, J. A., Thompson, D. M., & Wamsley, T. V. (2010). Numerical simulation of a low-lying barrier island's morphological response to Hurricane Katrina. *Coastal Engineering*, *57*, 985–995. https://doi.org/10.1016/j.coastaleng.2010.06.004

Lorenzo-Trueba, J., & Ashton, A. D. (2014). Rollover, drowning, and discontinuous retreat: Distinct modes of barrier response to sea-level rise arising from a simple morphodynamic model. *Journal of Geophysical Research: Earth Surface*, *119*, 779–801. https://doi.10.1002/2013JF002941

Masselink, G., Beetham, E., & Kench, P. D. (2020). Coral reef islands can accrete vertically in response to sea-level rise. *Science Advances*, *6*(24), eaay3656.

Masselink, G., Tuck, M., McCall, R., van Dongeren, A., Ford, M., & Kench, P. S. (2018). Physical and numerical modeling of infragravity wave generation and transformation on coral reef platforms. *Journal of Geophysical Research: Oceans*, *124*, 1410–1433. https://doi.org/10.1029/2018JC014411

Matias, A., Masselink, G., Castelle, B., Blenkinsopp, C., & Kroon, K. (2016). Measurements of morphodynamic and hydrodynamic overwash processes in a large-scale wave flume. *Coastal Engineering*, *113*, 33–46. http://dx.doi.org/10.1016/j.coastaleng.2015.08.005

Mattias, A., Williams, J., Ferreira, O., & Masselink, G. (2012). Barrier overwash. *Coastal Engineering*, *63*, 48–61. http://dx.doi.org/10.1016/j.coastaleng.2011.12.006

McCall, R.T., De Vries, J.V.T., Plant, N.G., Van Dongeren, A.R., Roelvink, J. A., Thompson, D. M., & Reniers, A. J. H. M. (2010). Two-dimensional time dependent hurricane overwash and erosion modeling at Santa Rosa Island. *Coastal Engineering*, *57*, 668–683. https://doi.org/10.1016/j.coastaleng.2010.02.006

McCall, R. T., Masselink, G., Poate, T. G., Roelvink, J. A., & Almeida, L. P. (2015). Modelling the morphodynamics of gravel beaches during storms with XBeach-G. *Coastal Engineering*, *103*, 52–66. http://dx.doi.org/10.1016/j.coastaleng.2015.06.002

McCall, R. T., Poate, T. G., MasselinkRoelvink, G. J. A., Almeida, L. P., Davidson, M., & Russell, P. E. (2014). Modelling storm hydrodynamics on gravel beaches with XBeach-G. *Coastal Engineering*, *91*, 231–250. http://dx.doi.org/10.1016/j.coastaleng.2014.06.007

Nielsen, P. (2002). Shear stress and sediment transport calculations for swash zone modelling. *Coastal Engineering*, *45*, 53–60. https://doi.org/10.1016/S0378-3839(01)00036-9

Orford, J., Jennings, R., & Pethick, J. (2003). *Extreme storm effect on gravel-dominated barriers* (pp.1–12). Paper presented at Proceedings Coastal Sediments'03.

Orford, J. D., Carter, R. W., Jennings, S. C., & Hinton, A. C. (1995). Processes and timescales by which a coastal gravel-dominated barrier responds geomorphologically to sea-level rise: Story head barrier, Nova Scotia. *Earth Surface Processes and Landforms*, *20*, 21–37. https://doi.org/10.1002/esp.3290200104

Pandolfi, J. M., Connolly, S. R., Marshall, D. J., & Cohen, A. L. (2011). Projecting coral reef futures under global warming and ocean acidification. *Science*, *333*, 418–422. https://doi.org/10.1126/science.1204794

Passeri, D. L., Long, J. W., Plant, N. G., Bilskie, M. V., & Hagen, S. C. (2018). The influence of bed friction variability due to land cover on storm-driven barrier island morphodynamics. *Coastal Engineering*, *132*, 82–94. https://doi.org/10.1016/j.coastaleng.2017.11.005

Pearson, S. G., Storlazzi, C. D., van Dongeren, A. R., Tissier, M. F. S., & Reniers, A. J. H. M. (2017). A Bayesian based system to assess wave-driven flooding hazards on coral reef-lined coasts. *Journal of Geophysical Research: Oceans*, *122*, 10099–10117. https://doi.org/10.1002/2017JC013204

Perry, C. T., Edinger, E. N., Kench, P. S., Murphy, G. N., Smithers, S. G., Steneck, R. S., & Mumby, P. J. (2012). Estimating rates of biologically driven coral reef framework production and erosion: A new census-based carbonate budget methodology and applications to the reefs of Bonaire. *Coral Reefs*, *31*, 853–868. https://doi.org/10.1007/s00338-012-0901-4

Perry, C.T., Alvarez-Filip, L., Graham, N. A., Mumby, P. J., Wilson, S. K., Kench, P. S., et al. (2018). Loss of coral reef growth capacity to track future increases in sea level. *Nature*, *558*, 396–400. https://doi.org/10.1038/s41586-018-0194-z

Perry, C. T., Kench, P. S., Smithers, S. G., Riegl, B., Yamano, H., & O'Leary, M. J. (2011). Implications of reef ecosystem change for the stability and maintenance of coral reef islands. *Global Change Biology*, *17*, 3679–3696. https://doi.org/10.1111/j.1365-2486.2011.02523.x

Poate, T., Masselink, G., & McCall, R. (2016). A new parameterisation for runup on gravel beaches. *Coastal Engineering*, *117*, 176–190. https://.doi.org/10.1016/j.coastaleng.2016.08.003

Pomeroy, A. W., & Van Rooijen, A. (2019). *The impact of fringing platform reefs on shoreline profiles*. Paper presented at Australasian Coasts and Ports 2019 Conference: Future directions from 40°S and beyond. Australia: Hobart.

Quataert, E., Storlazzi, C., van Dongeren, A., & McCall, R. (2020). The importance of explicitly modelling sea-swell waves for runup on reef-lined coasts. *Coastal Engineering*, *160*, 103704. https://doi.org/10.1016/j.coastaleng.2020.103704

Quataert, E., Storlazzi, C. D., van Rooijen, A., Cheriton, O., & van Dongeren, A. (2015). The influence of coral reefs and climate change on wave-driven flooding of tropical coastlines. *Geophysical Research Letters*, *42*, 6407–6415. https://doi.org/10.1002/2015GL064861

Roelvink, J. A., Reniers, A., van Dongeren, A. R., van Thiel de Vries, J. S. M., McCall, R., & Lescinski, J. (2009). Modeling storm impacts on beaches, dunes and barrier islands. *Coastal Engineering*, *56*, 1133–1152. https://doi.org/10.1016/j.coastaleng.2009.08.006

Roff, G., Zhao, J.-X., & Pandolfi, J. M. (2015). Rapid accretion of inshore reef slopes from the central Great Barrier Reef during the late Holocene. *Geology*, *43*, 343–346. https://doi.org/10.1130/G36478.1

Ryan, E. J., Hamner, K., & Kench, P. S. (2019). Massive corals maintain positive carbonate budget of a Maldivian upper reef platform despite major bleaching event. *Scientific Reports*, *9*, 1–11. https://doi.org/10.1038/s41598-019-42985-2

Sallenger, A. H. (2000). Storm impact scale for barrier islands. *Journal of Coastal Research*, *16*, 890–895.

Saunders, M., Albert, S., Roelfsema, C., Leon, J., Woodroffe, C., Phinn, S., & Mumby, P. (2016). Tectonic subsidence provides insight into possible coral reef futures under rapid sea-level rise. *Coral Reefs*, *35*, 155–167. https://doi.org/10.1007/s00338-015-1365-0

Scoffin, T. P. (1993). The geological effects of hurricanes on coral reefs and the interpretation of storm deposits. *Coral Reefs*, *12*, 203–221. https://doi.org/10.1007/BF00334480

Scopélitis, J., AndréfouëtPhinn, S. S., Done, T., & Chabanet, P. (2011). Coral colonisation of a shallow reef flat in response to rising sea level: quantification from 35 years of remote sensing data at Heron Island, Australia. *Coral Reefs*, *30*, 951. https://doi.org/10.1007/s00338-011-0774-y

Smallegan, S. M., Irish, J. L., Van Dongeren, A. R., & Den Bieman, J. P. (2016). Morphological response of a sandy barrier island with a buried seawall during Hurricane Sandy. *Coastal Engineering*, *110*, 102–110. https://doi.org/10.1016/j.coastaleng.2016.01.005

Smit, P., Stelling, G., Roelvink, J., Van Thiel de Vries, J., McCall, R., Van Dongeren, A., et al. (2010). *XBeach: Non-hydrostatic model: Validation, verification and model description*. Technical report Delft University of Technology.

Stockdon, H. F., Holman, R. A., Howd, P. A., Howd, P. A., & Sallenger, A. H. (2006). Empirical parameterization of setup, swash, and runup. *Coastal Engineering*, *53*, 573–588. https://doi.org/10.1016/j.coastaleng.2005.12.005

Stoddart, D. R., & Steers, J. A. (1977). The nature and origin of coral reef islands. In O. A. Jones, & R. Endean (Eds.), *Biology and geology of coral reefs*. (*IV*, pp. 59–105). New York, NY: Academic Press.

Storlazzi, C. D., Elias, E., Field, M. E., & Presto, M. K. (2011). Numerical modeling of the impact of sea-level rise on fringing coral reef hydrodynamics and sediment transport. *Coral Reefs*, *30*, 83–96. https://doi.org/10.1007/s00338-011-0723-9

Storlazzi, C.D., Gingerich, S. B., van Dongeren, A., Cheriton, O. M., Swarzenski, P. W., Quataert, E., et al. (2018). Most atolls will be uninhabitable by the mid-21st century because of sea-level rise exacerbating wave-driven flooding. *Science Advances*, *4*, eaap9741. https://doi.org/10.1126/sciadv.aap9741

Tuck, M., Ford, M. R., Masselink, G., & Kench, P. S. (2019). Physical modelling of reef island topographic response to rising sea levels. *Geomorphology*, *345*, 106833. https://doi.org/10.1016/j.geomorph.2019.106833

Tuck, M., Kench, P. S., Ford, M. R., & Masselink, G. (2019). Physical modelling of the response of reef islands to sea level rise. *Geology*, *47*, 803–806. https://doi.org/10.1130/G46362.1

van der Lugt, M. A., Quataert, E., van Dongeren, A., van Ormondt, M., & Sherwood, C. R. (2019). Morphodynamic modeling of the response of two barrier islands to Atlantic hurricane forcing., *Estuarine, Coastal and Shelf Science*, *229*, 106404. https://doi.org/10.1016/j.ecss.2019.106404

Van Woesik, R., & Cacciapaglia, C. W. (2018). Keeping up with sea-level rise: Carbonate production rates in Palau and Yap, western Pacific Ocean. *PLoS One*, *13*(5), e0197077. https://doi.org/10.1371/journal.pone.0197077

Van Woesik, R., & Cacciapaglia, C. W. (2019). Carbonate production of Micronesian reefs suppressed by thermal anomalies and Ancasthaster as sea-level rises. *PLoS One*, *14*(11), e0224887. https://doi.org/10.1371/journal.pone.0224887

van Woesik, R., Golbuu, Y., & Roff, G. (2015). Keep up or drown: adjustment of western Pacific coral reefs to sea-level rise in the 21st century. *Royal Society Open Science*, *2*, 150181. https://doi.org/10.1098/rsos.150181

Wadey, M., Brown, S., Nicholls, R., & Haigh, I. (2017). Coastal flooding in the Maldives: an assessment of historic events and their implications. *Natural Hazards*, *89*, 131–159. https://doi.org/10.1007/s11069-017-2957-5

Winter, G., Storlazzi, C., Vitousek, S., van Dongeren, A., McCall, R., Hoeke, R., et al. (2020). Steps to Develop Early Warning systems and future scenarios of storm wave-driven flooding along coral reef-lined coasts. *Frontiers in Marine Science*, *31*, 199. https://doi.org/10.3389/fmars.2020.00199

Woodroffe, C. D. (2008). Reef-island topography and the vulnerability of atolls to sea-level rise. *Global and Planetary Change*, *62*, 77–96. https://doi.org/10.1016/j.gloplacha.2007.11.001

Woodroffe, C. D., & Webster, J. M. (2014). Coral reefs and sea-level change. *Marine Geology*, *352*, 248–267. https://doi.org/10.1016/j.margeo.2013.12.006

Yates, K. K., Zawada, D. G., Smiley, N. A., & Tiling-Range, G. (2017). Divergence of seafloor elevation and sea level rise in coral reef ecosystems. *Biogeosciences*, *14*, 1739–1772. https://doi.org/10.5194/bg-14-1739-2017